Bcl-x_L regulates mitochondrial energetics by stabilizing the inner membrane potential

Ying-bei Chen,[1] Miguel A. Aon,[2] Yi-Te Hsu,[5] Lucian Soane,[6] Xinchen Teng,[1,6] J. Michael McCaffery,[9,10] Wen-Chih Cheng,[6] Bing Qi,[6] Hongmei Li,[11] Kambiz N. Alavian,[11] Margaret Dayhoff-Brannigan,[7] Shifa Zou,[6] Fernando J. Pineda,[6,8] Brian O'Rourke,[2] Young H. Ko,[3,4] Peter L. Pedersen,[3] Leonard K. Kaczmarek,[12] Elizabeth A. Jonas,[11] and J. Marie Hardwick[1,6,7]

[1]Department of Pharmacology and Molecular Sciences, [2]Institute of Molecular Cardiobiology, [3]Department of Biological Chemistry, and [4]Russell H. Morgan Department of Radiology and Radiological Science, Johns Hopkins School of Medicine, Baltimore, MD 21205
[5]Department of Biochemistry and Molecular Biology, Medical University of South Carolina, Charleston, SC 29425
[6]W. Harry Feinstone Department of Molecular Microbiology and Immunology, [7]Department of Biochemistry and Molecular Biology, and [8]Department of Biostatistics, Johns Hopkins Bloomberg School of Public Health, Baltimore, MD 21205
[9]Department of Biology and [10]Integrated Imaging Center, Johns Hopkins University, Baltimore, MD 21218
[11]Department of Internal Medicine and [12]Department of Pharmacology, Yale University School of Medicine, New Haven, CT 06520

Mammalian Bcl-x_L protein localizes to the outer mitochondrial membrane, where it inhibits apoptosis by binding Bax and inhibiting Bax-induced outer membrane permeabilization. Contrary to expectation, we found by electron microscopy and biochemical approaches that endogenous Bcl-x_L also localized to inner mitochondrial cristae. Two-photon microscopy of cultured neurons revealed large fluctuations in inner mitochondrial membrane potential when Bcl-x_L was genetically deleted or pharmacologically inhibited, indicating increased total ion flux into and out of mitochondria. Computational, biochemical, and genetic evidence indicated that Bcl-x_L reduces futile ion flux across the inner mitochondrial membrane to prevent a wasteful drain on cellular resources, thereby preventing an energetic crisis during stress. Given that F_1F_O–ATP synthase directly affects mitochondrial membrane potential and having identified the mitochondrial ATP synthase β subunit in a screen for Bcl-x_L–binding partners, we tested and found that Bcl-x_L failed to protect β subunit–deficient yeast. Thus, by bolstering mitochondrial energetic capacity, Bcl-x_L may contribute importantly to cell survival independently of other Bcl-2 family proteins.

Introduction

Bcl-x_L is an antiapoptotic Bcl-2 family member that is required for embryonic development and can contribute to cancer cell survival (Letai, 2008; Hardwick and Youle, 2009). The traditional viewpoint is that anti- and proapoptotic Bcl-2 family proteins actively engage each other to determine cell fate after a death stimulus (Galonek and Hardwick, 2006; Youle and Strasser, 2008). The best-characterized cell survival activity of Bcl-x_L is its ability to inhibit Bax-induced pores in the outer mitochondrial membrane (Billen et al., 2008). In this manner, Bcl-x_L prevents release of mitochondrial cytochrome *c* into the cytoplasm, where cytochrome *c* induces apoptosome formation to trigger caspase-dependent death of mammalian cells. Attention has been focused on the functional interactions and the binding specificities between anti- and proapoptotic Bcl-2–related proteins, leading to new therapeutic strategies (Oltersdorf et al., 2005).

The evolutionary conservation of Bcl-2–like proteins cannot be uniformly linked to apoptosis regulation (for example, the Bcl-2 homologues of *Drosophila melanogaster* and viruses; Bellows et al., 2002; Graham et al., 2008; Galindo et al., 2009). Many other binding partners have been reported for human Bcl-x_L, linking Bcl-x_L to other cellular processes including mitochondrial dynamics, energetics, and autophagy

Correspondence to J. Marie Hardwick: hardwick@jhu.edu

Abbreviations used in this paper: ANT, adenine nucleotide transporter; cKO, conditional knockout; DIV, day in vitro; ETC, electron transport chain; MS, mannitol sucrose; RIPA, radioimmunoprecipitation assay; ROI, region of interest; ROS, reactive oxygen species; shRNA, short hairpin RNA; TMRE, tetramethylrhodamine ethyl ester; TMRM, tetramethylrhodamine methyl ester.

Supplemental material can be found at:
http://doi.org/10.1083/jcb.201108059

The Rockefeller University Press $30.00
J. Cell Biol. Vol. 195 No. 2 263–276
www.jcb.org/cgi/doi/10.1083/jcb.201108059

(Vander Heiden et al., 2001; Levine et al., 2008; Li et al., 2008). Thus, Bcl-2 proteins may have alternative biochemical functions independent of their proapoptotic Bcl-2 family binding partners, or they may participate in other machineries before engaging classical apoptosis.

One nonapoptosis role of Bcl-2 family proteins in mammals and worms is regulation of mitochondrial fission and fusion (Karbowski et al., 2006; Berman et al., 2009; Montessuit et al., 2010; Hoppins et al., 2011). This role appears to contribute importantly to Bcl-x_L–induced mitochondrial localization at neuronal synapses, neuronal activity, and seizure behaviors (Fannjiang et al., 2003; Li et al., 2008). However, regulation of fission and fusion rates is not sufficient to explain the ability of endogenous and overexpressed Bcl-x_L to increase mitochondrial biomass (Berman et al., 2009). Therefore, we pursued alternative functions of Bcl-x_L in mitochondria. Consistent with an evolutionarily conserved function, Bcl-2 family proteins have been linked to control of mitochondrial energetics by regulating the voltage-dependent anion channel in the outer membrane or the adenine nucleotide transporter (ANT)/adenine nucleotide carrier in the inner membrane, which are the primary conduits through which ATP and ADP are exchanged between the cytosol and the mitochondrial matrix (Vander Heiden et al., 2001; Belzacq et al., 2003; Cheng et al., 2003). The relative contributions of antiapoptotic activity versus alternative functions of Bcl-x_L for overall cell survival are unclear.

The mitochondrial F_1F_O ATP synthase synthesizes ATP in the mitochondrial matrix using cytosolic ADP and phosphate as substrates (Hong and Pedersen, 2004). This process requires a potential across the inner mitochondrial membrane that is generated by pumping out protons via the electron transport chain (ETC; or respiratory chain) fueled by NADH. Reentry of protons into the mitochondrial matrix via the F_O ring (oligomycin-sensitive fraction) embedded in the inner membrane drives rotation of the central stalk against the catalytic F_1, a ring of three α and three β subunits (Walker and Dickson, 2006). In this manner, proton flux through F_O is coupled to ATP synthesis. Because mitochondrial membrane potential is required for essential functions other than ATP synthesis, there are alternative strategies for building a potential. Reversal of the F_1F_O ATP synthase hydrolyzes cytoplasmic ATP produced by glycolysis, reversing the flow of protons through F_O to stabilize a potential (Nicholls and Ferguson, 2002; Abramov et al., 2007). A membrane potential is also required for mitochondrial fusion, and depolarization of the potential leads to Parkin-dependent mitophagy (Narendra et al., 2008; Twig et al., 2008). Although mitochondrial energetics are linked to mitochondrial morphology changes, the details are complex (Benard and Rossignol, 2008).

By analyzing *bcl-x*–deficient neurons, we uncovered a new function of Bcl-x_L. We found that Bcl-x_L can localize to the inner mitochondrial membrane/matrix, which is contrary to current opinion. Importantly, Bcl-x_L is required to stabilize the membrane potential across the inner mitochondrial membrane. By decreasing excess ion flux across the inner mitochondrial membrane, Bcl-x_L increases overall energetic efficiency, which is consistent with the limited reserve capacity of *bcl-x*–deficient neurons and their susceptibility to cell death. This function of Bcl-x_L involves the mitochondrial F_1F_O ATP synthase.

Results

Defective control of mitochondrial membrane potential in *bcl-x*–deficient neurons

To explore the function of Bcl-x_L in healthy neurons, several mitochondrial parameters were analyzed by two-photon laser-scanning fluorescence microscopy, comparing control and *bcl-x* conditional knockout (cKO) cortical neuron cultures (Berman et al., 2009). Both unfloxed and *bcl-x*–floxed littermates express neuron-specific knockin NEX-Cre recombinase starting around embryonic day 12 (E12) to delete *bcl-x*. Staining for Cre recombinase serves as a positive marker for the survival of *bcl-x*–deficient (and control unfloxed) cortical neurons (Fig. 1 A; Berman et al., 2009). Mitochondrial membrane potential ($\Delta\Psi_m$) was assessed in immature cortical cultures with the potentiometric dye tetramethylrhodamine methyl ester (TMRM; nonquench mode), revealing higher fluorescence intensity in the mitochondria-enriched regions of *bcl-x* knockout cortical neurons (Fig. 1, B and C [left]). This is not a result of increased mitochondrial biomass because *bcl-x*–deficient neurons have lower, not higher, mitochondrial biomass in these and other cell types based on several criteria (Kowaltowski et al., 2002; Berman et al., 2009). Thus, it appears that *bcl-x* deficiency may result in a higher mitochondrial membrane potential.

In respiring cells, three direct mechanisms (Fig. 1 D, dashed boxes) of proton flux across the inner membrane (Fig. 1 D, blue arrows) are main determinants of $\Delta\Psi_m$: (1) the ETC, (2) the F_1F_O ATP synthase, and (3) uncoupling proteins or other molecularly undefined leak mechanisms (protons not used for ATP synthesis; Nicholls and Ferguson, 2002). To further explore these parameters in *bcl-x* knockout neurons, reactive oxygen species (ROS) production by the ETC was assessed in the same mitochondrial areas where TMRM was evaluated. Unexpectedly, *bcl-x* knockout neurons have lower mitochondrial ROS. This suggests either a high rate of electron flow through the respiratory chain or that *bcl-x* knockout neurons are more dependent on glycolysis than on mitochondrial respiration for energy production (Fig. 1, A and B). The same mitochondrial areas of *bcl-x* knockout neurons have modestly higher mitochondrial NAD(P)H levels, which is consistent with an earlier study (Schwartz et al., 2007). Higher levels of the complex I substrate NADH indicate more than adequate supplies of NADH either because the respiratory chain is inactive or other metabolic processes are altered, such as decreased anaplerosis (Abramov et al., 2007; Cheng et al., 2011). However, no inherent defects in respiratory chain activity were detected when complexes I–IV, II–IV, and IV were assessed by measuring oxygen consumption in isolated brain mitochondria (Fig. S1, A and B). The relative contributions of glycolysis versus the mitochondrial F_1F_O ATP synthase to the levels of total cellular ATP

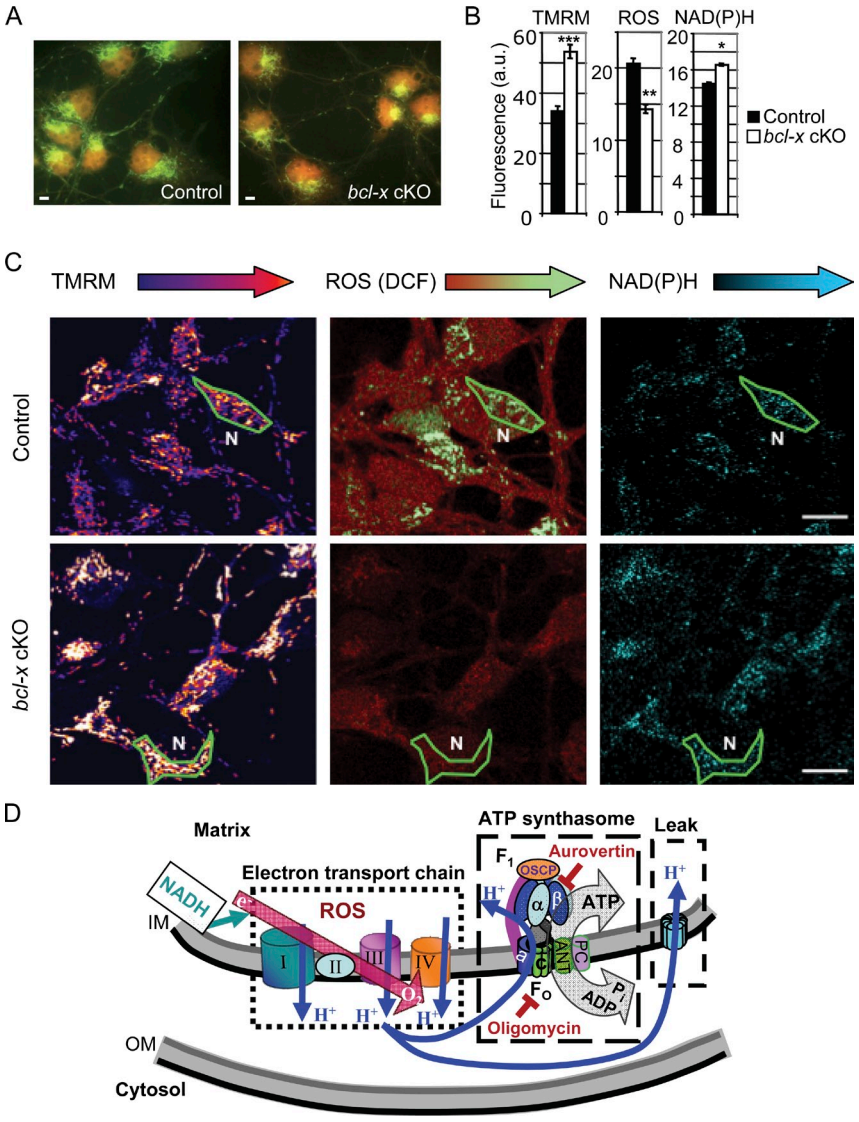

Figure 1. **Altered mitochondrial parameters in *bcl-x*–deficient neurons.** (A) Immunofluorescence microscopy of control (*bcl-x*$^{+/flox}$;*NEX*$^{+/cre}$) and cKO (*bcl-x*$^{flox/flox}$;*NEX*$^{+/cre}$) cortical cultures (DIV6) stained with anti–cytochrome *c* (green; 7H8.2C12 [1:80; BD] and goat anti–mouse Alexa Fluor 488 [Invitrogen]) to detect mitochondria and costained for Cre recombinase (red; anti-Cre [1:2,000; EMD] and Cy3 goat anti–rabbit [1:1,000; Jackson ImmunoResearch Laboratories, Inc.). Images were captured with a real-time camera (Diagnostic Instruments, Inc.) and a microscope (Eclipse E800; Nikon). Bars, 4 µm. (B) Summary of mean fluorescence intensities ± SEM from two-photon microscopy images of live cortical cultures recorded simultaneously in three channels to assess $\Delta\Psi_m$ (100 nM TMRM), ROS accumulation (2 µM CM-DCF), and NAD(P)H (intrinsic fluorescence) in one mitochondria-enriched ROI per cell for multiple cells (control, $n = 50$; cKO, $n = 56$) from multiple cultures (control, $n = 9$; cKO, $n = 11$), with each culture prepared from a different embryo. a.u., arbitrary unit. Student's *t* test was used; *, $P < 10^{-6}$; **, $P < 10^{-10}$; ***, $P < 10^{-12}$. (C) Examples of two-photon microscopy images marking example ROI. Fluorescence intensity is scaled with pseudocolors (filled arrows). N, nucleus. Bars, 10 µm. (D) A diagram of three major determinants of mitochondrial membrane potential (dashed boxes). Electron flow from NADH to O_2 (red arrow) via the ETC complexes (I–IV), proton (H^+) paths across the membrane (blue arrows), ATP/ADP + Pi exchange via ANT and phosphate carrier (PC; gray arrow), and inner mitochondrial membrane (IM) and outer mitochondrial membrane (OM). OSCP, oligomycin sensitivity–conferring protein.

were also similar between *bcl-x* knockout and control cultures. ATP levels (relative to total protein) were slightly reduced in the *bcl-x* knockout cortical cultures, though this was a result in part of 15% lower cell viability compared with controls (Fig. S1, C and D). In sum, no defects were detected to explain the altered mitochondrial parameters of *bcl-x* knockout neurons.

Localization of endogenous Bcl-x_L includes mitochondrial cristae

To pursue the role of Bcl-x_L in regulating mitochondrial parameters, we determined the subcellular localization of endogenous Bcl-x_L protein in neurons of the brain. Endogenous Bcl-x_L in HeLa cells resides predominantly in the cytosol as a homodimer and translocates to mitochondria via its C-terminal transmembrane domain after a death stimulus (Jeong et al., 2004). However, crude fractionation of mouse cortex suggests that a significant proportion of endogenous Bcl-x_L localizes to mitochondria in the brain (Fig. 2 A), which is consistent with an earlier finding (Soane et al., 2008). Deletion of *bcl-x* (except in interneurons and glial cells where NEX-Cre is not expressed; Berman et al., 2009) did not significantly alter other mitochondrial markers (Fig. 2 A).

Immunogold EM was used to more precisely determine the subcellular localization of endogenous Bcl-x_L in tissue slices of mouse brain hippocampus. Approximately 90% of gold-labeled anti–Bcl-x_L (BioCarta) is associated with membranes, and at least half of these membranes (54%) can be clearly identified as mitochondria (Fig. 2, B and C). Surprisingly, most of the mitochondrial staining was inside mitochondria, where the colabeled ATP synthase β subunit was also found (Figs. 2 [B and C] and S2). The frequency of labeled mitochondria with inner membrane/matrix Bcl-x_L gold label (58%) argues strongly against the possibility of contamination from the outer membrane as a result of edge skimming, folding of the slice preparation, or random background. Gold particles on mitochondria were also detected in polar clusters (Fig. 2 C, arrowheads) and on membranes adjacent to mitochondria, possibly marking mitochondrial fission/fusion sites or where the outer mitochondrial membrane may be tethered to the ER (Fig. 2 C, line arrows), though patchy staining can reflect the uneven epitope accessibility in ultrathin cryosections.

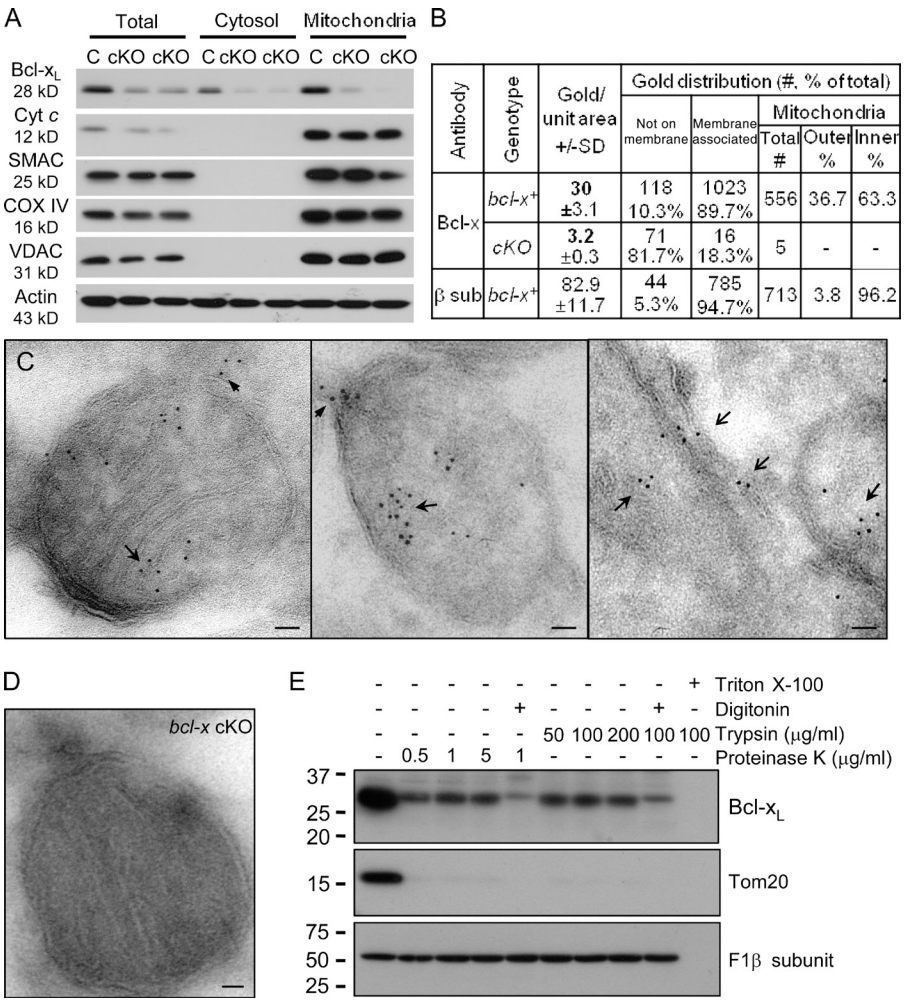

Figure 2. **Submitochondrial localization of endogenous Bcl-x_L.** (A) Immunoblots of total cell lysates (clarified), cytosolic fractions, and heavy membranes prepared from dissected cortexes pooled from three 3-d-old mice per sample. Blots were probed with antibodies to Bcl-x_L (1:1,000; provided by L. Boise), cytochrome *c* (Cyt *c*; 7H8.2C12 [1:1,000]), cytochrome oxidase subunit IV (COX IV; 1:1,000; Invitrogen), SMAC (1:1,000; Invitrogen), voltage-dependent anion channel (VDAC; 1:1,000; EMD), actin (1:1,000; MP Biomedicals), and UCP-2 (6525 [1:100; Santa Cruz Biotechnology, Inc.]). A representative of three independent experiments is shown. (B) Summary of immunogold EM staining for Bcl-x_L and ATP synthase β proteins in control and cKO mouse brain representing three independent experiments. (C) EM of microdissected CA1 hippocampus (where CA1 synapses onto CA3) from mouse brains stained with gold-labeled Bcl-x_L antibody detects Bcl-x_L on mitochondrial inner membranes/cristae (black arrows), outer membrane polar clusters (arrowheads), and adjacent membranes (line arrows). Bars, 0.1 µm. (D) Immunogold staining of *bcl-x* cKO CA1 mouse brain prepared in parallel as in C. Bar, 0.1 µm. (E) Immunoblot analysis of Percoll-purified nonsynaptic adult rat brain mitochondria. Mitochondria were incubated with the indicated proteases (for 30 min) with or without 0.01% digitonin to permeabilize the outer membrane and were blotted for Bcl-x_L (1:1,000; Abcam), Tom20 (11415 [1:2,000; Santa Cruz Biotechnology, Inc.]), and ATP synthase β subunit (A21351 [1:1,000; Invitrogen]).

Importantly, this staining is specific for Bcl-x_L based on multiple parallel preparations of the same brain regions from *bcl-x* cKO mice, in which total anti–Bcl-x_L immunogold label was reduced by ∼90%, and mitochondrial Bcl-x_L gold was reduced ∼99% (Fig. 2, B and D).

To support these findings, protease susceptibility of Bcl-x_L was analyzed in purified rat brain mitochondria. Unlike the outer membrane protein Tom20, a portion of Bcl-x_L (Abcam antibody) is resistant to proteases even after treatment with digitonin to permeabilize the cholesterol-containing outer membrane (Fig. 2 E). As expected, matrix-localized β subunit was protected from digestion until addition of Triton X-100 to disrupt the inner membrane, when both Bcl-x_L and β subunit were completely digested. The proportion of Bcl-x_L protected from proteases by the inner membrane can be higher depending on the antibody used (Fig. S3). We conclude that a portion of endogenous Bcl-x_L localizes to the inner mitochondrial membrane and/or matrix. These findings are in sharp contrast to the widely held view that Bcl-2 family proteins are localized only to the cytoplasmic side of the outer, not inner, mitochondrial membranes, though inner membrane localization of Bcl-x_L and Bcl-2 has been previously reported (Hockenbery et al., 1990; Kharbanda et al., 1997; Motoyama et al., 1998; Gotow et al., 2000; Belzacq et al., 2003).

Biochemical purification of Bcl-x_L with inner membrane components

The possibility that Bcl-x_L regulates mitochondrial membrane potential by acting at the inner mitochondrial membrane led us to revisit our earlier yeast two-hybrid screen (Chau et al., 2000). Seeking to identify prosurvival functions distinct from anti-apoptotic functions of Bcl-x_L in an unbiased screen, the BH1 domain mutant of Bcl-x_L (mt1; F131V/D133A), which inhibits cell death without binding prodeath family members Bax or Bak (Cheng et al., 1996), was used to screen a human B cell library (Chau et al., 2000). Among the six hits, we identified an unexpected Bcl-x_L–binding partner, the β subunit of the mitochondrial F_1F_O ATP synthase. This interaction was confirmed in a secondary yeast two-hybrid screen in which the β subunit interacted with wild-type Bcl-x_L and Bcl-2 but did not interact with mutants lacking antideath activity (Bcl-x_L mt7 and mt8) and did not interact with Bax or Bak (Fig. 3 A). Because Bcl-x_L mt1 could potentially inhibit mammalian cell death by binding BH3-only proteins (Billen et al., 2008), we assayed the function of mt1 and mt8 in yeast, which lack Bcl-2 and BH3-only proteins. Bcl-x_L mt1 but not mt8 protected yeast from dose-dependent cell death (Fig. 3 B).

An independent biochemical purification scheme also identified the β subunit as the prominent binding partner of

endogenous Bcl-x_L. WEHI 7.1 membrane preparations were solubilized with CHAPS to avoid detergent-induced dimerization with Bax during extract preparation (Hsu and Youle, 1997). Bcl-x_L–containing complexes were purified by sequential ion exchange and immunoaffinity chromatography followed by preparative SDS-PAGE (Fig. 3 D). The only major Coomassie-stained species copurifying with Bcl-x_L was ~54 kD. Direct sequencing of two tryptic peptides derived from this extracted band yielded exact matches with the human/mouse F_1F_O ATP synthase β-subunit residues 244–253 (NDLYHEMIES) and 389–404 (IAELGIYPAVDPLDST).

A screen of 80 detergents yielded a strategy for purifying enzymatically active F_1F_O ATP synthase from mitoplasts isolated from rat liver mitochondria for the purpose of 3D structure determination (Ko et al., 2003). Immunoblot analyses of these preparations revealed monomeric Bcl-x_L, which decreased in abundance with purification as a band approximately the size of Bcl-x_L dimers was enriched with purification (Fig. 3 C). Detergents likely induced SDS-stable dimers of Bcl-x_L, which are frequently encountered with purified Bcl-x_L (O'Neill et al., 2006). On parallel blots, both Bcl-x_L bands were eliminated when the antibody was preadsorbed with recombinant Bcl-x_L protein, indicating that Bcl-x_L is enriched in highly purified preparations of the ATP synthase from liver. To determine whether Bcl-x_L is monomeric or present in larger complexes inside cells, CHAPS-solubilized lysates were separated by column chromatography, revealing that all of the Bcl-x_L was in complexes >70 kD that overlap fractions containing the β subunit (Fig. 3 E). An association of Bcl-2 with the F_1F_O ATP synthase has also been observed by the laboratories of J. Downward (London Research Institute, London, England, UK), Y. Tsujimoto (Osaka University, Osaka, Japan), and S. Korsmeyer and G. Linette (Washington University in St. Louis, St. Louis, MO; personal communication).

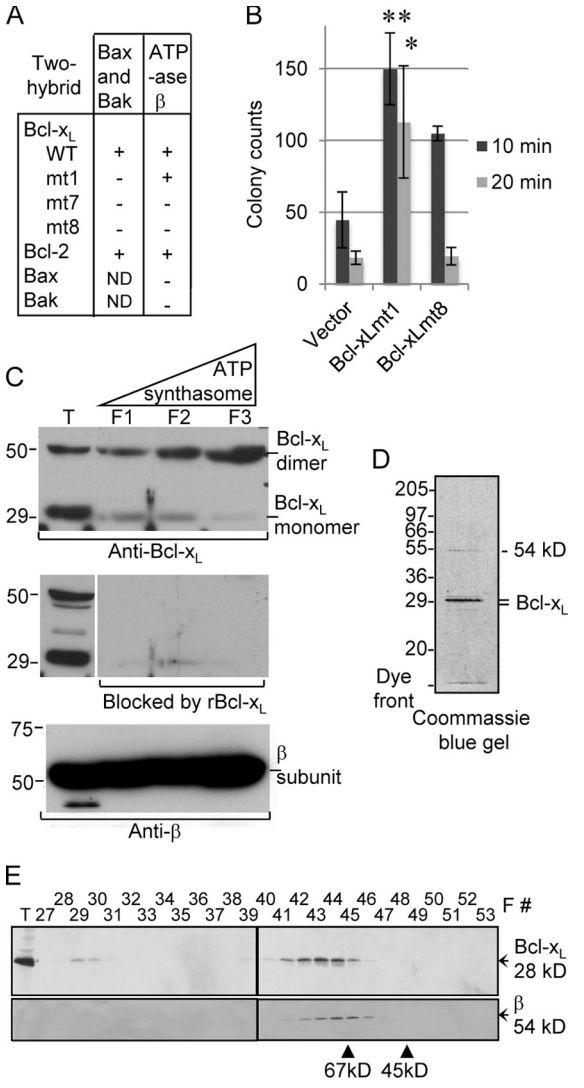

Figure 3. **Bcl-x_L association with inner mitochondrial membrane components.** (A) Summary of yeast two-hybrid interactions between BCL-2 family proteins and the ATP synthase β subunit, including wild-type (WT) and Bcl-x_L mutants mt1 (F131V/D133A), mt7 (V135A/N136I/W137L), and mt8 (G138E/R139L/I140N). (B) Yeast (BY4741) transformed with the indicated plasmids were heat ramp treated and presented as colony counts from four determinations in two independent experiments. Data are presented as the mean ± SEM. Student's *t* test was used; *, P = 0.012 compared with control; **, P = 0.001. (C) Immunoblots for Bcl-x_L (provided by L. Boise) or β subunit in total rat liver mitochondria (T), inner membrane vesicles (F1), and highly purified ATP synthasomes (F2 and F3) of increasing purity (Ko et al., 2003). The replicate blot in the middle was probed with Bcl-x_L antibody preincubated with recombinant Bcl-x_L (rBcl-x_L) protein purified from *Escherichia coli* (lanes F1–F3 only). (D) Coomassie blue–stained preparative SDS gel of final purification step for Bcl-x_L–binding partners from WEHI 7.1 cells. (E) Immunoblots for Bcl-x_L and β subunit in size column chromatography fractions (F) and total lysates (T). Eluted size markers are indicated.

Membrane potential fluctuations in *bcl-x*–deficient mitochondria

Because the mitochondrial F_1F_O ATP synthase is an important control point for proton flux across the inner mitochondrial membrane, mitochondrial membrane potential was further evaluated by time-lapse imaging (3.5-s intervals). TMRM intensity in mitochondria-enriched regions fluctuates modestly in control neurons, which is consistent with an earlier study (Vergun et al., 2003). However, *bcl-x*–deficient neurons exhibited a striking fluctuation in TMRM fluorescence intensity over irregular intervals in time (Fig. 4 A), across a single *bcl-x* knockout cell (Fig. 4 B), and in individual mitochondria (Fig. 4 C). Thus, the increase in mean mitochondrial potential in *bcl-x*–deficient neurons (Fig. 1 B) represents the mean of a time-varying potential that fluctuates predominantly to higher (more negative) potentials than controls. Therefore, the presence of Bcl-x_L stabilizes the inner mitochondrial membrane potential.

Because Bcl-x_L can bind to the inositol triphosphate receptor in the ER to regulate calcium gating by the inositol triphosphate receptor (White et al., 2005), we investigated a role for calcium in mitochondrial membrane potential fluctuation. We found that basal cytosolic calcium levels were uniformly steady in cultured *bcl-x* knockout and control cortical neurons (Fig. 4 D). Although compiled data indicate a small but significant calcium elevation in *bcl-x* knockout neurons, fluctuations in potential appear not to be controlled by paired fluctuations in cytosolic calcium.

To investigate the possibility that Bcl-x_L has a direct role in stabilizing the mitochondrial membrane potential, tetramethylrhodamine ethyl ester (TMRE) fluorescence intensity was

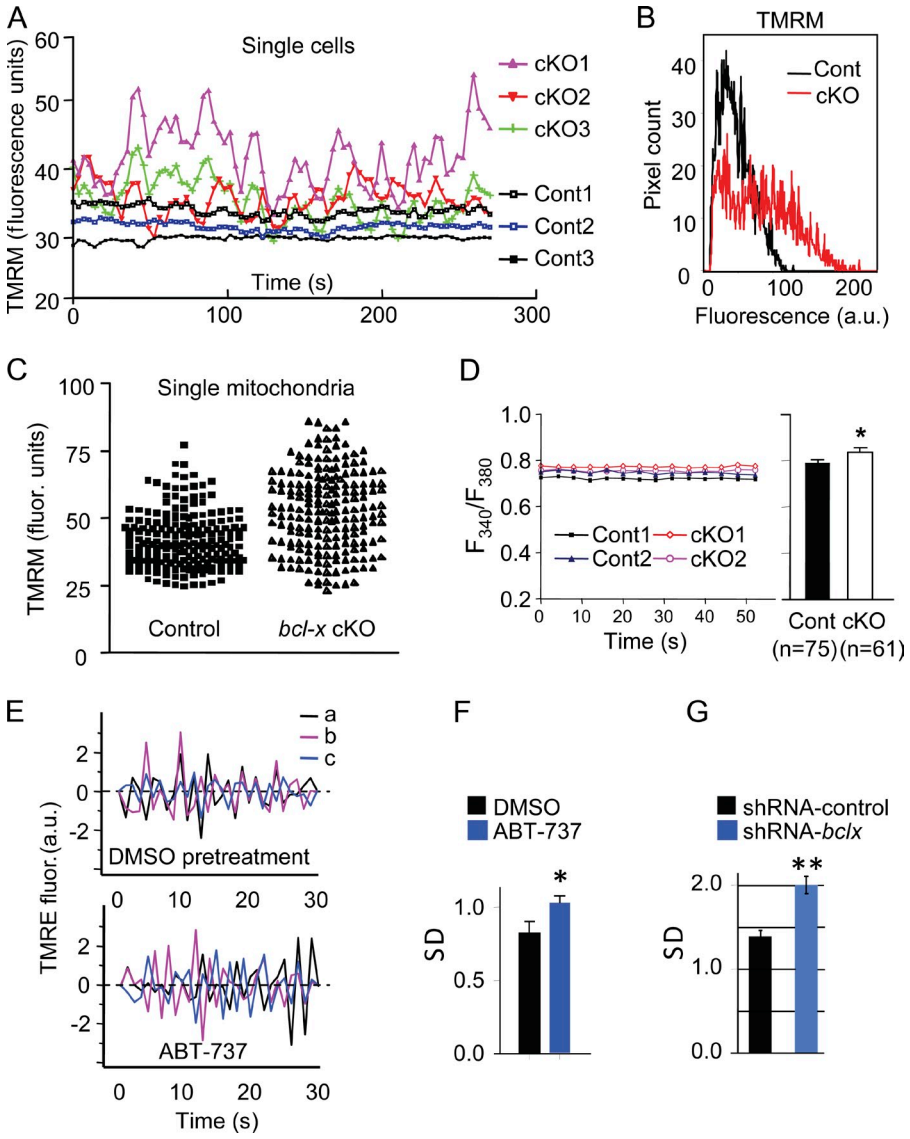

Figure 4. **Bcl-x_L–deficient mitochondria have fluctuating membrane potentials.** (A) Continuous recordings (3.5-s intervals) of TMRM intensities per ROI of individual cortical neurons for at least 250 s (DIV4–5; Fig. 1). Traces are representative of multiple neurons in three independent experiments. (B) Fluorescence intensity (arbitrary units [a.u.]) of TMRM stain per pixel was determined for the marked mitochondria-rich region of a single neuron in *bcl-x*–deficient (cKO) and control (Cont) cultures shown in Fig. 1 C. (C) SDs were calculated for mean TMRM fluorescence intensities per pixel for 200 individual mitochondria derived from 20 different cells per genotype monitored every 2.5 s for at least 90 s. Each symbol represents one mitochondrion. An F-test for variance comparing control and *bcl-x*–deficient neuronal mitochondria was performed; $P < 0.0001$. (D) Continuous recordings of intracellular calcium levels at 4-s intervals in DIV3–4 cortical neurons. Initial intracellular calcium levels from four independent experiments are graphed. *, $P = 0.039$. (E) Mitochondrial membrane potential fluctuation increases with ABT-737. Fluorescence intensities were measured in small puncta (estimated to be one mitochondrion) near the soma in cultured rat hippocampal neurons (DIV14–16) stained with 5 nM TMRE. Relative fluorescence intensities (collected at 1/s) for the same puncta/mitochondria treated with 0.1% DMSO before and after addition of 1 µM ABT-737 (in 0.1% DMSO) for 10 min are shown. (F) SDs of TMRE intensity measurements as in E; data are for 30 measurements for each of 12 puncta in six cells in two independent experiments and are similar to three additional experiments with protocol variations. Paired *t* test was used; *, $P = 0.02$. (G) SD of TMRE as in F, except 4 d after transfection with shRNA vector with scrambled ($n = 10$) or *bcl-x*–specific shRNAs ($n = 17$). Fluorescent images were taken every 3 s for 8 min. Paired *t* test was used; **, $P = 0.00027$. (F and G) Data are presented as the mean ± SD.

monitored in cultured hippocampal neurons treated only briefly with ABT-737, a specific inhibitor of Bcl-x_L designed to fit the binding pocket on Bcl-x_L and block its antiapoptotic function (Oltersdorf et al., 2005). Individual mitochondria exhibited greater fluctuations in TMRE fluorescence intensity after only 10 min of ABT-737 (in 0.1% DMSO) compared with DMSO alone (Fig. 4, E and F). To confirm the specificity of ABT-737, hippocampal neurons expressing scrambled or *bcl-x*–specific short hairpin RNA (shRNA) were monitored for TMRE fluorescence intensity in time (Fig. S4), and the SD of fluorescence intensities was significantly greater for the *bcl-x* knockdown than the control (Fig. 4 G). These data again suggest that Bcl-x_L stabilizes the mitochondrial membrane potential by limiting total ion flux across the mitochondrial membrane.

Bcl-x_L stabilizes the mitochondrial membrane potential to conserve energy

It is known that when any chemical system is not at thermodynamic equilibrium, as is the case for respiring mitochondria, the occurrence of persistent fluctuations or oscillations can only be maintained by expending energy (Nicolis and Prigogine, 1977). Moreover, the additional time-dependent flux of ions across the inner membrane that drives these fluctuations in potential can result in an overall ion flux (both inward and outward directions) that is greater than what is required simply to maintain a nonfluctuating membrane potential at a steady negative value. Thus, the fluctuations in mitochondrial membrane potential in *bcl-x* knockouts imply that more energy is required to maintain ion gradients across the inner membrane. To illustrate this concept, we constructed a simple numerical model to investigate the effect of fluctuations on the dissipation of ion gradients across the mitochondrial membrane. A vesicle (1 µm in diameter) was used to represent a mitochondrion (Fig. 5 A). This vesicle was equipped with active ion pumps (Fig. 5 A, b) capable of pumping out protons/ions (approximating the respiratory chain) to build a negative potential (−180 mV) and with ion channels (Fig. 5 A, a) that can partially dissipate this potential by allowing ions to reenter the vesicle (approximating the F_1F_O ATP synthase and nonproductive leaks). We first modeled steady-state conditions in which the inward flux and

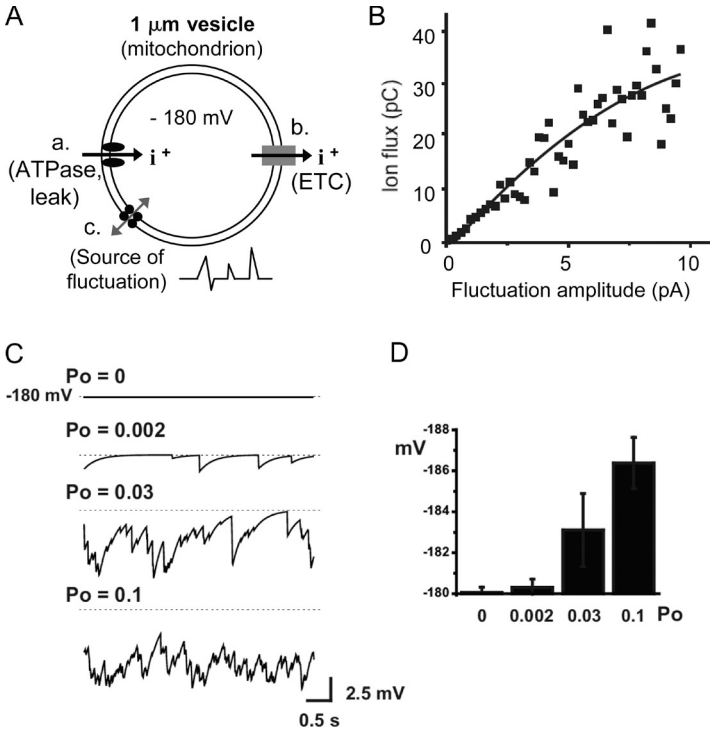

Figure 5. **Bcl-x_L stabilizes the mitochondrial membrane potential to conserve energy.** (A) A simplified model of ion flux across the inner mitochondrial membrane. Ions may enter or leave the matrix through leakage channels at point a (e.g., the F_1F_O ATP synthase through which protons enter the mitochondrial matrix), and overall stability and membrane potential are maintained by active pumps at point b (e.g., the ETC). The double arrow represents the source of fluctuation in potential. (B) Numerical simulations of the additional ion flux that occurs as a result of fluctuations in membrane potential using the 1-μm membrane vesicle model in A. An external perturbation with a fixed amplitude between 0 and 10 pA (5-ms duration) was allowed to occur randomly with a mean interval of 1 s, and the total ion flux was integrated over 20-s periods. The graph plots the increase in total integrated flux that results from fluctuations of increasing amplitude. (C) Numerical simulations of changes in mitochondrial inner membrane potential produced by stochastic opening of a nonselective cation channel. No openings occur when probability of channel opening (Po) equals 0, and the membrane is maintained at a steady level (−180 mV; dashed lines). Indicated opening rates of the channel produce fluctuations in membrane potential accompanied by net hyperpolarization (more negative potentials). (D) Mean ± SD of membrane potentials for traces in C.

outward flux of ions are exactly matched in time, and the membrane potential does not fluctuate in amplitude. These conditions approximate the steady-state conditions of mitochondria in wild-type cells. Next, we modeled fluctuations in membrane potential by introducing small currents across the vesicle membrane (Fig. 5 A, c). These small currents (set arbitrarily at 5 ms with a fixed amplitude between 0 and 10 pA) were allowed to occur randomly (averaging 1/s) to drive fluctuations in the potential across the vesicle membrane. To assess the effects of these external current amplitudes (Fig. 5 A, c), we measured the magnitude of total ion flux through the pumps (Fig. 5 A, a) and the channels (Fig. 5 A, b). In all cases, the total amount of ion flux (measured in picocoulombs) was increased when current fluctuations were introduced and was further increased with increasing external current amplitude (Fig. 5 B). The additional amount of ion movement (Fig. 5 A, a and b) produced by the small transient current fluctuations (Fig. 5 A, c) represents a futile dissipation of the ion gradient that has to be balanced by pump activity to restore the mean membrane potential. Thus, Bcl-x_L could improve mitochondrial energetics simply by preventing futile ion flux.

Collectively, our results suggest the possibility that Bcl-x_L regulates an inner mitochondrial membrane ion-conducting channel and that this channel has an increased probability of opening in the absence of Bcl-x_L. This increased channel opening (analogous to point c in Fig. 5 A) could result in the increased membrane potential fluctuations observed in the *bcl-x* knockout. To investigate the effects of such a Bcl-x_L–regulated channel on mitochondrial membrane potential fluctuations, we made a second computational model that more closely represents known properties of the inner mitochondrial membrane. This enabled us to test explicitly the effect of very brief transient openings of a nonselective inner membrane channel on the mitochondrial membrane potential measured over time. A vesicle (1.5 μm in diameter) was equipped with a proton pump and a proton leak pathway as in Fig. 5 A (a and b). The steady-state proton concentration of the mitochondrion was further regulated by a fixed proton buffer and a proton–cation exchange pathway (Garlid and Paucek, 2003). Finally, we introduced a nonselective cation channel representing the one regulated by Bcl-x_L, which is permeable to both protons and to other cations and has a reversal potential of 0 mV (Lam et al., 1998; Vander Heiden et al., 2001; Alavian et al., 2011). Opening of the nonselective cation channel (mean open time of 0.33 ms) was allowed to occur stochastically with different opening probabilities of 0–0.1. We found that opening of the nonselective channel produced fluctuations in the membrane potential that increased with increased probability of channel opening (Fig. 5, C and D). The simulation further reveals that the very brief increases in internal proton concentration produced by influx through the channel resulted in proton pump activation, resulting in an overall hyperpolarization of the membrane as the frequency of channel openings increased (Fig. 5, C and D). This is consistent with transient hyperpolarization of mitochondria in *bcl-x* knockout cells as a result of overshooting by the respiratory chain after the channel opens.

Draining resources in Bcl-x_L–deficient neurons

Our vesicle models predict that the increased membrane leakiness (productive and nonproductive ion flux) across the inner mitochondrial membrane in *bcl-x*–deficient neurons will result in decreased energetic performance. To test this prediction, cultured *bcl-x* cKO and control cortical neurons were energetically stressed by the addition of mitochondrial ATP synthase inhibitors and analyzed for ATP levels and for mitochondrial parameters by two-photon microscopy. Extensive genetic and

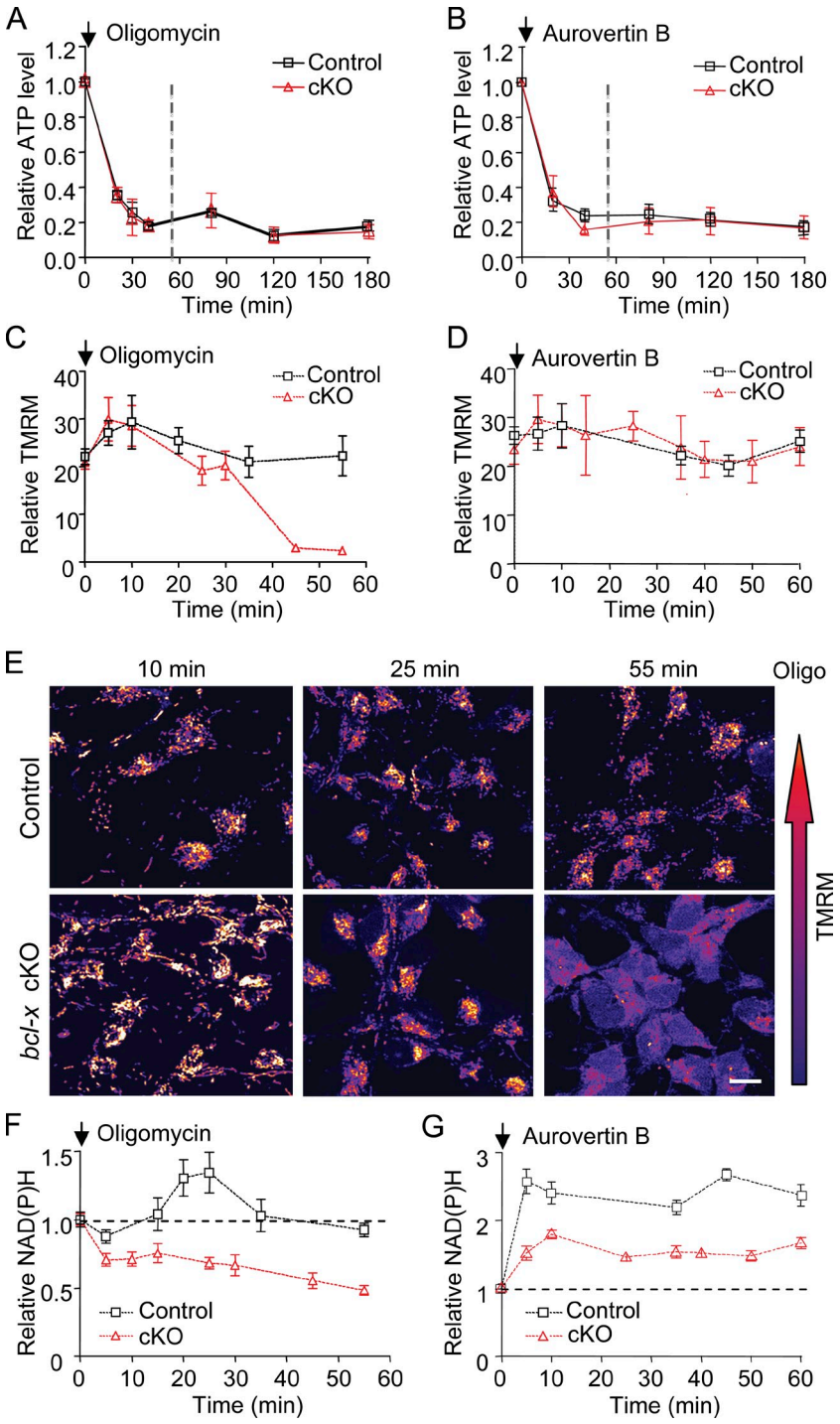

Figure 6. **Leaky energetics in Bcl-x_L–deficient mitochondria.** (A and B) Total ATP levels corrected for total protein in paired DIV3–6 cortical cultures after addition of 5 µg/ml oligomycin (control [*n* = 8] and cKO [*n* = 7] at each of six time points in three independent experiments) or 20 µg/ml aurovertin B (control [*n* = 5] and cKO [*n* = 4] at each of six time points from two independent experiments). Vertical dashed lines mark the time frame evaluated for TMRM fluorescence in C and D. Data are presented as the mean ± SEM. (C and D) Time course of TMRM fluorescence intensities (mean ± SEM) after addition of 5 µg/ml oligomycin. Analyses of 15–35 neurons from three to five fields per genotype per time point are presented, and results are representative of five similar independent experiments. Parallel experiments were performed with 20 µg/ml F_1 inhibitor aurovertin B (*n* = 13–35 cells from two to three fields at each time point; total of 136 control and 193 cKO cells) from two independent experiments. (E) Two-photon microscopy images of cortical neurons (DIV4) stained with 100 nM TMRM to assess $\Delta\Psi_m$ as described for Fig. 1 C after addition of 6 nM oligomycin (Oligo.). A representative of five independent experiments is shown. Bar, 10 µm. (F and G) Relative NAD(P)H levels were determined in the same cellular subregions analyzed in C and D, as described for but not included in Fig. 1 B. Horizontal dashed lines mark starting NAD(P)H levels. Data are presented as relative ratios for direct comparisons. Mean ± SEM is represented, and values are the same as in C and D.

biochemical evidence indicates that oligomycin inhibits mitochondrial ATP synthesis by acting on F_O to disrupt the proton path (Walker and Dickson, 2006), and a crystal structure reveals that aurovertin B inhibits the enzymatic F_1 subunit by binding near the ATP-binding site on β subunit (van Raaij et al., 1996). Treatment with oligomycin or with aurovertin B caused cellular ATP levels to decline similarly in control and knockout neurons (Fig. 6, A and B). Therefore, the F_1F_O ATP synthase was an important contributor to ATP production and concomitant dissipation of membrane potential in both genotypes before treatment.

In contrast to controls, *bcl-x*–deficient cortical neurons consistently underwent delayed mitochondrial depolarization 30–45 min after the addition of oligomycin (Fig. 6, C and E). Consistent with an energy-wasting crisis unique to *bcl-x*–deficient neurons, oligomycin also causes mitochondrial NAD(P)H levels to decline to ∼50% of pretreatment levels in <1 h, whereas NAD(P)H levels rebound and stabilize after oligomycin treatment in controls (Fig. 6 F). These results suggest that *bcl-x*–deficient mitochondria continue to deplete the substrate of complex I, as would be expected for a leaky mitochondrial membrane that allows the respiratory chain to continue running.

Consistent with this conclusion, rates of oxygen uptake by cells decrease with overexpression of Bcl-x_L and increase with shRNA knockdown of Bcl-x_L (Alavian et al., 2011). NAD(P)H depletion and membrane depolarization were not simply a result of inhibition of mitochondrial ATP synthesis because NAD(P)H levels and membrane potential were sustained for at least 1 h after aurovertin B treatment, although at lower steady-state levels relative to controls (see Discussion; Fig. 6 G). To verify that depletion of NAD(P)H and mitochondrial depolarization is not simply a marker of cell death, oligomycin was washed away from depolarized *bcl-x*–deficient neurons in a flow chamber. Upon washout, we observed simultaneous increases in NAD(P)H levels and TMRM intensity, indicating cell recovery (Fig. 7 A). The evidence presented suggests that Bcl-x_L increases the efficiency of mitochondrial energetics by decreasing inner membrane leakiness, thereby preventing membrane potential fluctuations and the resulting energy deficits (Fig. 7 B).

Bcl-x_L requires the β subunit for antideath activity in yeast

To test whether Bcl-x_L increases cell survival through a functional interaction with F_1F_O ATP synthase and independently of any other Bcl-2 family members, we tested the ability of human Bcl-x_L to inhibit cell death of yeast lacking β subunit (Δ*atp2*) of the F_1F_O ATP synthase. Using a novel heat ramp cell death assay (Teng et al., 2011), we found that Bcl-x_L failed to protect yeast in which the ATP2 gene was deleted. In contrast, Bcl-x_L protected yeast with mutations in both the mitochondrial fission protein *FIS1* and *WHI2*, which lack mitochondrial fission and have respiratory function defects (*Δfis1**; Figs. 7 C and S5; Fannjiang et al., 2004; Cheng et al., 2008). Yeast have no recognizable Bcl-2 family members or BH3-only proteins yet have a highly conserved F_1F_O ATP synthase. Our results indicate that Bcl-x_L promotes cell survival through an interaction with the ATP synthase.

Discussion

Our evidence indicates that endogenous Bcl-x_L prevents a futile ion flux across the mitochondrial inner membrane, thereby preventing pronounced irregular fluctuations in mitochondrial membrane potential observed in *bcl-x* knockout cells. The additional energy required for fueling excessive ion flux across the mitochondrial membrane would place *bcl-x*–deficient cells at a distinct disadvantage during cell stress. Unable to sustain a potential across a more leaky inner membrane, *bcl-x*–deficient mitochondria depolarize and subsequently die. Prominent localization of endogenous Bcl-x_L with the inner mitochondrial membrane is consistent with a close link between Bcl-x_L and the membrane leak channels. Copurification of Bcl-x_L with the F_1F_O ATP synthase raises the possibility that a novel leak channel could be within the ATP synthase itself or a functionally interacting component. This function of Bcl-x_L can be expected to alter many other aspects of mitochondrial and cellular physiology, though, like many mitochondrial proteins, the mechanism by which Bcl-x_L enters mitochondria is not known.

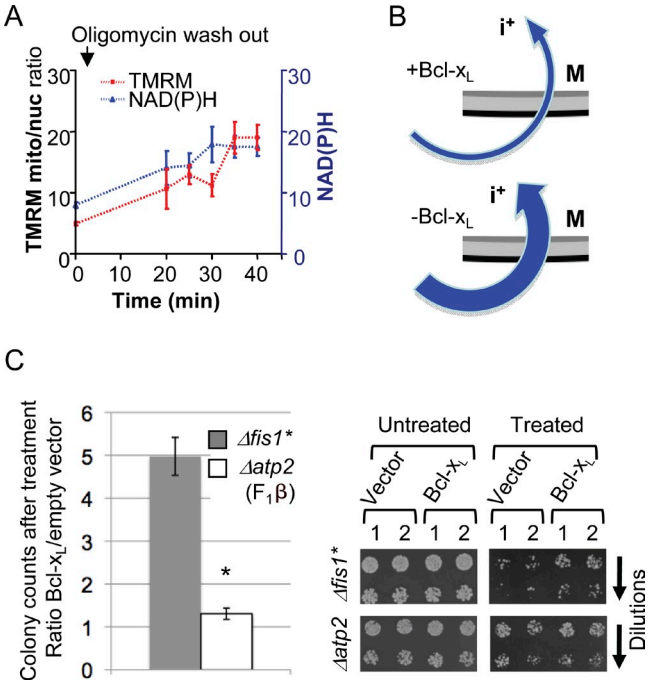

Figure 7. **Nonapoptotic function of Bcl-x_L.** (A) Two-photon microscopy of *bcl-x*–deficient cultured neurons was performed as described for Fig. 1 B, except using a flow chamber. The measurements shown begin with the flow of oligomycin-free medium after 40 min of 5 µg/ml oligomycin (n = 4–11 per time point per genotype). Data are presented as the mean ± SD. (B) A model depicting an increase in membrane leak in the absence of Bcl-x_L. M, matrix. (C) Heat ramp cell death assay of yeast strains with mutant *ATP2* or *FIS1/whi2-1* (Cheng et al., 2008; Teng et al., 2011). Representative images of yeast growth are shown; arrows indicate fivefold dilutions. Data are presented as mean ± SD for four independent strains per plasmid, each tested in duplicate in each of two independent experiments and plotted as the ratio of colony numbers for Bcl-x_L/empty vector (*FIS1/whi2*, n = 10; *ATP2*, n = 16). Student's t test was used; *, $P = 5.7 \times 10^{-10}$.

Bcl-x_L inhibits mitochondrial membrane leakiness

These findings are consistent with a conceptually simple mechanism in which Bcl-x_L acts at the inner mitochondrial membrane to close a molecularly undefined leak, thereby preventing large swings in membrane potential. This could be achieved if Bcl-x_L directly closes the leak channel. Our computational models predict that opening of this Bcl-x_L–inhibited leak channel results in membrane potential fluctuations, which is consistent with fluctuations observed in *bcl-x*–deficient cells. The models further predict that the large fluctuations are a result of transient overcompensations by the respiratory chain, which is consistent with the observed transient hyperpolarizations in *bcl-x*–deficient cells. Our numerical simulations also suggest that the greater total flux of ions across the mitochondrial inner membrane in *bcl-x*–deficient mitochondria requires more energy to maintain ionic homeostasis, analogous to other fluctuating or oscillating biochemical systems (Kaczmarek, 1976). Even if the additional ion flux in *bcl-x*–deficient mitochondria was coupled to ATP synthesis by F_1F_O, additional energy would be required to move ions out of the matrix when the potential is fluctuating compared with a steady state with little or no fluctuations. Our simulations are consistent with the notion that the stabilizing effect of Bcl-x_L on inner mitochondrial membrane potential

contributes importantly to the efficiency of energy production. An expected negative consequence of excess ion flux is that a sudden deficit in nutrients or a sudden increase in energy demand cannot be readily satisfied by an inefficient system.

Seemingly contrary to these findings, recombinant Bcl-x_L can induce ion channel activity in outer mitochondrial membranes and synthetic bilayers, although these channels are smaller than those formed by the related proapoptotic Bax protein (Lam et al., 1998; Basañez et al., 2002). Thus, the ion-conducting activity of Bcl-x_L may not be related to the Bcl-x_L functions under study here. However, more complex scenarios remain possible where Bcl-x_L channels open to correct other ion-conducting activities in the inner membrane, thereby preventing large swings in potential. Though the detailed molecular events remain unclear, our conclusions are supported by patch clamp recordings of mitochondrial inner membrane vesicles with Bcl-x_L (Alavian et al., 2011). It is conceivable that the Bcl-x_L–inhibited mitochondrial leak channel is related to the Bax pores that trigger apoptosis, except Bax pores are not known to occur in inner membranes (Billen et al., 2008). The capacity of a non–Bax/Bak-binding mutant of Bcl-x_L (mt1) to interact with the F_1 β subunit and to inhibit cell death in mammalian cells argues against this possibility. Furthermore, Bcl-x_L can inhibit cell death in wild-type yeast, which lack Bcl-2 family and BH3-only proteins, but Bcl-x_L cannot protect yeast lacking F_1 β, which shares 89% amino acid sequence homology with humans. The inner membrane function and the antideath function of Bcl-x_L appear to be separable biochemical events (e.g., Fig. 7 A). However, yet unknown nonapoptotic activities of Bax/Bak could be involved, potentially those that regulate neuronal activity or inhibit neuronal cell death in vivo (Lewis et al., 1999; Fannjiang et al., 2003). Furthermore, Bcl-x_L was recently reported to regulate acetyl-CoA levels in a Bax/Bak-independent manner (Yi et al., 2011).

Given the unexpected finding that mitochondrial ROS levels in *bcl-x*–deficient cells are lower than controls, our data are not consistent with Bcl-x_L–mediated leak closure serving to reduce ROS levels (Jastroch et al., 2010). To the contrary, the leakier/fluctuating membrane potential could be expected to increase oxygen consumption in *bcl-x*–deficient cells, which is consistent with reduced oxygen consumption in Bcl-x_L–overexpressing cells (Alavian et al., 2011).

Implications for the F_1F_o ATP synthase

Because Bcl-x_L is not found in the 3D structures of F_1F_o ATP synthase, we considered other potential functions for partnering. Given a structural resemblance between Bcl-x_L and Diphtheria toxin, a polypeptide translocator, we considered that Bcl-x_L could facilitate entry of the β subunit into mitochondria. However, we found that *bcl-x*–deficient mitochondria appear to have normal levels of β subunit. Bcl-x_L could interact with fully assembled ATP synthase or participate in the assembly process, which requires many factors not present in active complexes (Rak et al., 2011). Alternatively, the effects of Bcl-x_L on membrane curvature could influence the ATP synthase (Basañez et al., 2002; Paumard et al., 2002).

Our biochemical and pharmacological analyses are consistent with a Bcl-x_L–regulated leak mechanism involving the F_1F_o ATP synthase. However, the differential effects of two F_1F_o inhibitors are somewhat puzzling. Both aurovertin B (acting on F_1) and oligomycin (acting on F_O) block ATPase/synthase activity and proton movement through F_o because of the coupling between F_1 and F_o. Yet, only aurovertin B inhibited mitochondrial depolarization in *bcl-x*–deficient cells, possibly by triggering closure of the leak channel by binding the β subunit (van Raaij et al., 1996). In contrast, the Bcl-x_L–regulated leak channel appears to be oligomycin resistant, though it is not clear whether this is the long sought-after leak channel that explains continued mitochondrial respiration with oligomycin treatment (Nicholls and Ferguson, 2002). We speculate that the F_1F_O ATP synthase is involved in leaking ions and that the regulation of this function is defective in *bcl-x*–deficient neurons. These studies further extend the long-standing link between Bcl-2 family proteins and the ATP synthase (Matsuyama et al., 1998; Vander Heiden et al., 2001; Belzacq et al., 2003).

Materials and methods

Primary cortical neuron cultures

Conditional *bcl-x* knockout cortical neuron cultures were prepared separately from individual E16.5 mouse embryos as previously described (Berman et al., 2009). Wild-type and floxed *bcl-x* mice/embryos were distinguished using PCR primers 5′-GCCACCTCATCAGTCGGG-3′ and 5′-TCAGAAGCCGCAATATCCC-C-3′. The *NEX-CRE* locus was identified with primers 5′-TCTTTTTCATGTGCTCTTGG-3′ and 5′-CCGCATAACC-AGTGAAACAG-3′, and the wild-type allele was identified with 5′-CAAGTTGTCCTTCGAGGAAAGAGC-3′ and 5′-GATACAGACAAG-AGGGAAGGG-3′. All experiments were performed on density-matched cultures. All animal procedures were approved by the Animal Care and Use Committee. For immunofluorescence microscopy, cortical neuron cultures were quickly washed with Locke's buffer (154 mM NaCl, 5.6 mM KCl, 2.3 mM $CaCl_2$, 1.0 mM $MgCl_2$, 5 mM Hepes, and 10 mM glucose, pH 7.4), fixed for 15 min in 4% PFA, permeabilized for 5 min with 0.2% Triton X-100, blocked for 30 min at RT with 5% normal goat serum, and incubated with primary antibodies at 4°C overnight followed by 1 h at RT with secondary antibodies.

Two-photon laser-scanning microscopy

Potentiometric dye TMRM, which accumulates in the matrix according to its Nernst potential, was used at 100 nM (the lowest workable concentration; nonquench mode verified with carbonyl cyanide-*p*-trifluoromethoxyphenylhydrazone) to monitor mitochondrial membrane potential $\Delta\Psi_m$. Accumulation of ROS was monitored simultaneously with 2 µM CM-H_2DCFDA (5-(-6)-chloromethyl-2′,7′-dichlorohydrofluorescein diacetate). Fluorescence probes were loaded into cortical neuron cultures (3–5 days in vitro [DIV3–5]) for at least 20 min, and images were recorded using a two-photon laser-scanning microscope (MRC-1024MP; Bio-Rad Laboratories) with an excitation at 740 nm (Tsunami Ti:Sa laser; Spectra-Physics) to measure fluorescence intensity of TMRM (605 ± 25 nm), CM-DCF (525 ± 25 nm), and intrinsic autofluorescence of endogenous NADH/NADPH (<490 nm; Aon et al., 2003). For single recordings, three to five fields per culture dish were imaged in immediate succession. For time-lapse recordings, images of the same field were captured every 3.5 s for up to 5 min using 50% laser intensity to limit photo damage to live samples. Region of interests (ROIs) were drawn and analyzed using ImageJ (National Institutes of Health) for all neurons per image. Mean fluorescence intensity per pixel in each ROI at the three emission wavelengths was calculated as arbitrary fluorescence units. Background from cell-free areas was subtracted for each wavelength. Photodamage-induced fluctuations specifically in knockout cells is unlikely, as fluctuations are evident at the earliest time points and with single-photon microscopes (Fig. 4), and treatment with antioxidant *N*-acetyl cysteine does not inhibit depolarization.

Mitochondrial respiration

Mouse forebrain mitochondria were isolated from littermates of control and cKO mice (postnatal day 2–7 [P2–P7]) by modification of a standard protocol (Rosenthal et al., 1987). Mitochondria (primarily nonsynaptosomal) were

prepared as previously described for subcellular fractionation and were further washed with mannitol sucrose (MS) buffer (without EGTA). Rates of oxygen consumption by purified mitochondria (0.5 mg/ml) were measured with a Clark-type oxygen electrode (Hansatech Instruments Limited) in KCl buffer (125 mM KCl, 20 mM Trizma base, 2 mM potassium phosphate, and 1 mM $MgCl_2$, pH 7.2) plus substrates (Fig. S1 A), 1 mM $MgCl_2$, and 0.25 mM EGTA and were calculated in nanomoles of O_2 per mg protein per minute based on a KCl medium oxygen content of 195 nmol/ml O_2 at 30°C.

Crude subcellular fractionation

Cerebral cortexes from P3 mice were rapidly dissected, minced on ice in 2 ml MS-EGTA buffer (225 mM mannitol, 75 mM sucrose, 250 µM EGTA, 1 mg/ml fatty acid–free BSA, and 5 mM Hepes, pH 7.4), and homogenized with 15 strokes in a 2 ml Dounce. The cortical suspension was clarified (at 2,800 *g* for 3 min at 4°C), and mitochondria were collected by centrifugation (15,000 *g* for 8 min), gently resuspended in MS-EGTA, and recentrifuged (for 10 min). The pellet was lysed in 100 µl MS buffer + 1% NP-40, and the supernatant was centrifuged at 100,000 *g* for 30 min to clarify the cytosolic fraction.

Immunoblot analyses

Mouse cerebral cortex was dissected on ice and passed 15 times through a 25-guage needle in 3 vol of radioimmunoprecipitation assay (RIPA) lysis buffer (50 mM Tris, 1% NP-40, 150 mM NaCl, and 1 mM EDTA, pH 7.4) plus 1 mM NaF, 1 mM Na_3VO_4 (sodium orthovanadate and phosphatase inhibitor), and protease inhibitors (PMSF, leupeptin, pepstatin, and aprotinin). Cultured cortical neurons were washed quickly with Locke's buffer and lysed in 150 µl of RIPA buffer. 50-µg lysates were separated by SDS-PAGE and blotted with specific antibodies (see figure legends).

Immuno-EM

Immunogold labeling of ultrathin cryosections was performed as previously described (McCaffery and Farquhar, 1995). Tissues from both genotypes were fixed in 4% PFA diluted in PBS, pH 7.4, for 15 min followed by 8% PFA for 1 h at RT. Samples were cryoprotected in 2.3 M sucrose plus 20% polyvinylpyrrolidone (for 1 h), mounted on aluminum cryopins, and frozen in liquid N_2. 80-nm ultrathin cryosections cut on a microtome (Ultracut T; Reichert) equipped with an FCS cryostage were collected onto 300 mesh formvar/carbon-coated nickel grids. Grids were passed through several drops of PBS plus 2.5% FCS and 0.01 M glycine, pH 7.4, blocked in 10% FCS, and incubated overnight with mixed primary antibodies against ATP synthase β subunit (BD) and/or anti–Bcl-$x_{L/S}$ antibody, each at ∼10 µg/ml. Washed grids were incubated for 2 h with one or both secondary antibody gold conjugates (1:50; Jackson ImmunoResearch Laboratories, Inc.). Grids were washed several times, first with PBS and then with double-distilled H_2O. Grids were embedded (3.2% polyvinyl alcohol [molecular mass of 10 kD], 0.2% methyl cellulose [400 cps], and 0.2% uranyl acetate) and observed on a transmission electron microscope (EM 410; Philips Research Eindhoven), and images were collected with a digital camera (SIS Megaview III; Olympus). Figures were assembled in Photoshop (Adobe) with only linear adjustments in brightness and contrast.

Subfractionation of mitochondria and protease treatment

Nonsynaptic brain mitochondria were isolated from adult male Sprague Dawley rats (weights of 300–350 g) by using a Percoll gradient centrifugation method as previously described (Kristian et al., 2007). In brief, rat forebrains were removed and homogenized in isolation medium (225 mM mannitol, 75 mM sucrose, 5 mM Hepes, 1 mM EGTA, 225 mM mannitol, 75 mM sucrose, 5 mM Hepes, and 1 mg/ml fatty acid–free BSA, pH 7.4, at 4°C). The resulting homogenate was centrifuged at 1,300 *g* for 3 min. The supernatant containing mitochondria was collected, and the pellet was resuspended and recentrifuged at 1,300 *g*. The pooled supernatants were then centrifuged for 10 min at 16,000 *g*. The crude mitochondrial pellet was resuspended in 15% Percoll and layered on top of a 40/20% Percoll gradient and then centrifuged for 12 min at 21,000 *g*. Nonsynaptic mitochondria were collected from the interface of the two bottom layers, diluted with isolation medium, and centrifuged at 16,000 *g* for 8 min. The purified mitochondrial pellet was resuspended in isolation medium and kept on ice until use. Protein concentration of mitochondrial samples was determined by using the BCA assay (Thermo Fisher Scientific) and BSA as standards. Mitochondrial protease digestion assays were performed by incubating freshly isolated mitochondria (1 mg/ml in isolation medium containing 1 mM $MgCl_2$) for 30 min at 37°C with either 0.2–25 µg/ml Proteinase K or 25–200 µg/ml Trypsin. 0.01% digitonin was used to permeabilize the outer mitochondrial membrane. The reactions were stopped by addition of a protease inhibitor cocktail (Thermo Fisher Scientific), and then mitochondria were collected by centrifugation (16,000 *g* for 10 min at 4°C), and the mitochondrial pellets were lysed in RIPA lysis buffer (30 mM Tris-HCl, pH 7.4, 0.15 M NaCl, 1% NP-40, 0.1% SDS, 0.5% sodium deoxycholate, 1 mM EDTA, 1 mM DTT, and 2 mM $MgCl_2$) containing protease inhibitors. The sensitivity of various mitochondrial proteins to protease digestion was then examined by immunoblot analysis using the following antibodies: anti–Bcl-x_L (ab2568, 1:1,000; Abcam), anti–cytochrome *c* (clone 7H8.2C12, 1:1,000; Thermo Fisher Scientific), anti-Tom20 (sc-11415, 1:2,000; Santa Cruz Biotechnology, Inc.), and anti–ATP synthase β subunit (1:1,000). The ATP synthasome fractions used are as previously described (Ko et al., 2003) and were solubilized in lithium dodecyl sulfate for separation by SDS-PAGE.

Biochemical purification of Bcl-x_L–binding partners

WEHI 7.1 cells (∼20 ml packed pellet) were lysed in 200 ml of hypotonic buffer (37.5 mM NaCl and 10 mM Hepes, pH 7.4) plus 25 µg/ml PMSF using a Dounce homogenizer. The membrane pellet (at 23,000 *g* for 30 min) was solubilized in 300 ml of isotonic buffer (150 mM NaCl and 10 mM Hepes, pH 7.4) plus 1% CHAPS and was clarified by centrifugation (for 15 min at 15,000 *g*). The supernatant was loaded onto a 10-ml trimethylaminoethyl anion exchange column and washed with 10 column volumes of isotonic buffer with 0.5% CHAPS, and bound proteins were eluted with a salt gradient (Bcl-x_L eluted at 0.35 M NaCl). Bcl-x_L–containing fractions were immunoaffinity purified with 1 ml anti–murine Bcl-x_L antibody 7D9 (Hsu et al., 2003) bound to beads (2 mg antibody/ml Sepharose beads) for 3 h at 4°C. Beads were washed with isotonic buffer with 0.5% CHAPS, and Bcl-x_L–containing complexes were eluted with 3 ml of 0.1 M acetic acid + 0.3% CHAPS. The sample was neutralized with 0.4 ml of 1 M Tris (pH 8.0), concentrated (Centricon-30), and separated by preparative SDS-PAGE.

Gel filtration of membrane-associated Bcl-x_L

10^8 HeLa cells stably expressing Bcl-x_L (Hou et al., 2003) were lysed by Dounce homogenization in hypotonic buffer. The membrane pellet (at 31,000 *g* for 30 min) was solubilized in 3 ml of isotonic buffer plus 1% CHAPS and clarified by centrifugation (at 31,000 *g* for 15 min). The supernatant (0.4 ml) was loaded onto a 38-ml Superdex 200 gel filtration column (GE Healthcare) precalibrated with 67 kD BSA, 45 kD ovalbumin, and 24 kD chymotrypsinogen. 0.4-ml column fractions containing Bcl-x_L were identified by immunoblot analysis with monoclonal 2H12 (Hsu and Youle, 1997).

TMRE fluctuation in hippocampal neurons

Dissociated rat hippocampal neurons were prepared from E18 embryos and plated on poly-L-lysine–coated dishes in Neurobasal medium with B27 (Invitrogen; Li et al., 2008). Mature (DIV14–16) cultures were incubated at 37°C in recording buffer (5 mM KCl, 110 mM NaCl, 2 mM $MgCl_2$, 10 mM glucose, 10 mM Hepes, 2 mM $CaCl_2$, pH 7.4, and 310 mOsm) containing TMRE (5 nM final). Individual puncta containing mitochondria at the base of a dendrite near the soma were outlined and measured by averaging 4 × 4 pixels as previously described (Li et al., 2008). Fluorescent images were collected (1/s for 30 s) with fixed exposure times (300 ms) using an inverted microscope (Axiovert 200; Carl Zeiss) with a 63× oil objective. Background fluorescence was subtracted for each image, and data were analyzed using AxioVision software (version 4.3; Carl Zeiss). For analysis of SDs, a straight baseline was subtracted from each graphed line using OriginLab 8.0 software to eliminate any artifacts due to slight organelle movement during imaging.

Calcium measurement

Mouse cortical neurons (DIV3–5) grown on 15-mm coverslips were loaded with 2 µM cell-permeable Fura-2 acetoxymethyl ester at 37°C for 30 min, washed with culture medium, and incubated at 37°C for 20–30 min to allow complete hydrolysis of acetoxymethyl ester. Coverslips were mounted on a AttoFluor system (Carl Zeiss) and continuously infused with Locke's buffer. Cells were sequentially excited at 340 nm/380 nm, and fluorescence intensities (510 nm) were determined for individual neurons from images captured at ∼4-s intervals. The 340:380 ratios were converted to nanomoles Ca^{2+} using a video imaging system (Intracellular Imaging Inc.) and commercial reference standards (Invitrogen) by the formula $[Ca^{2+}]_i = K_d ([R - R_{min}]/[R_{max} - R])(F_{max}/F_{min})$, where R equals the ratio of 510-nm emission intensities excited at 340 nm relative to 380 nm, R_{min} equals the ratio at zero free Ca^{2+}, R_{max} equals the ratio at saturating Ca^{2+} (39 µM), F_{min} equals the fluorescence intensity excited at 380 nm for zero free Ca^{2+}, and F_{max} equals the fluorescence intensity excited at 380 nm in saturating Ca^{2+}.

Numerical simulations

To estimate the flux of ions in the model vesicle (Fig. 5 A), we integrated the equation $CdV/dt = I_{ch} + I_{f(t)}$, where V is the membrane potential across the vesicle, C represents the capacitance of the vesicle, I_{ch} is the ionic current flowing through the channel in the membrane, and $I_{f(t)}$ is an additional fluctuating current that is applied across the membrane. I_{ch} was defined by the equation $I_{ch} = g_L(V_0 - V)$, where g_L is the conductance of the membrane and, under steady-state conditions, provides a membrane potential of −180 mV (V_0 = −180 mV). $I_{f(t)}$ was either fixed at 0 or was allowed to fluctuate from 0 to a value $I_F max$ for 5-ms periods. These fluctuations occurred randomly with a mean period of 1 s. In different simulations, the value of $I_F max$ was increased from 0.01 to 10 pA. Equations were integrated for a time span of 20 s, and the ion flux for the entire period was calculated in picocoulombs. Activity of pumps was not simulated explicitly in these models but was incorporated implicitly because the reversal potential for ion flux (V_0 = −180 mV) was held fixed during the simulations. Parameters for the simulations were C = 0.314 picofarads and g_L = 3.14 picosiemens.

For the second model, we tested the effects of a nonselective cation channel on the membrane potential across the inner mitochondrial membrane. For simplicity, we included a fixed proton buffer and an electroneutral proton–cation (K^+) exchange pathway (Garlid and Paucek, 2003) such that, in the absence of any other channel activity, this model has a steady-state internal proton concentration of 20 nM (pH 7.7) and a membrane potential of −180 mV, as is typical for many mitochondria.

We integrated the following pair of coupled stochastic differential equations:

$$\frac{dH_t}{dt} = A_v \begin{pmatrix} \left(g_H + \lambda(t)\, g_{CHAN}\right) \times \left(-68 \log_{10}\left(\frac{H_{in}}{H_{out}}\right) - V\right) \\ -k_R H_{in}\left(200 + V\right) + k_X\left(H_{out} - H_{in}\right) \end{pmatrix} \text{ and}$$

$$\frac{dV}{dt} = \frac{1}{C}\begin{pmatrix} -\left(\lambda(t)\, g_{CHAN} + g_L\right)V + g_H\left(-68 \log_{10}\left(\frac{H_{in}}{H_{out}}\right) - V\right) \\ -k_R H_{in}\left(200 + V\right) \end{pmatrix}.$$

H_t is the total bound and unbound concentration of protons in the vesicle, and V is the voltage across the membrane. H_{out} is the H^+ concentration outside the vesicle and was fixed at 40 nM, whereas H_{in}, the concentration of free protons in the vesicle, was related to the value of H_t and to B, the concentration of H^+ buffer in the vesicle, by the following quadratic equation:

$$H_{in} = \frac{-K_{eq} - B + H_{tot} + \sqrt{\left(K_{eq} + B - H_{tot}\right)^2 + 4K_{eq}H_{tot}}}{2}.$$

Here, $B = 5 \times 10^{-3}$ mM, and $K_{eq} = 2.3 \times 10^{-5}$ mM.

The constant A_v was equal to $(1.036 \times 10^4)/W$, where W is the volume of the vesicle (1.767 mm^2). The capacitance of the vesicle C was 5×10^{-9} nanofarads. The values for g_H (the basal proton leak), g_L (the basal leak of cations), and g_{CHAN} (the conductance of the nonselective cation channel) were 5, 5.55×10^{-6}, and 5×10^{-4} picosiemens, respectively. The values for k_R (the rate constant for H^+ pumping out of the vesicle) and k_X (the rate of electroneutral cation/H^+ exchange) were 2.5 and 5×10^{-5} ms^{-1}, respectively.

I(t) is a stochastic function that takes on the value of 1 or 0 depending on whether the nonselective cation channel is open or closed. The open probability, P_0, of the channel was determined by the rate constants for channel opening (k_f) and closing (k_b) and was given by the following relation:

$$P_o = \frac{k_f}{k_f + k_b}.$$

The value of k_b was fixed at 0.3 ms^{-1}, which provided a mean open time of 3.33 ms. In the simulations of Fig. 5 (C and D), the values of k_f were set at 0, 0.0005, 0.0101, and 0335 ms^{-1}, providing mean open probabilities of 0, 0.0017, 0.323, and 0.1004.

ATP measurements

Cortical cultures were harvested as for immunoblot analysis plus a phosphatase inhibitor; mouse cortex lysates were supplemented with 50 mM atractyloside. Samples were analyzed immediately, or time points were frozen instantly and analyzed together. Protein concentration/sample (BCA assay) and fresh ATP standards (0, 25 µM, 5 µM, 500 nM, 50 nM, and 5 nM) were used to calibrate every experiment.

Yeast cell death assay

Overnight cultures of yeast strains (*MATa, his3Δ1, leu2Δ0, met15Δ0, ura3Δ0,* and *yfg::KanMX4*; Invitrogen) transformed with modified pRS-PGK vector without/with human Bcl-x_L were diluted and grown to midlog phase (synthetic complete–uracil medium) and plated before and after a heat ramp treatment to trigger cell death (30–40°C in 2 min, 40–51°C in 10 min, and held at 51°C for 5 min; Teng et al., 2011). Both the *ATP2* and *FIS1** knockout strains are more sensitive to cell death than wild type, in which Bcl-x_L also protects (Fannjiang et al., 2004). For immunoblot analyses, lysates were prepared from overnight cultures in lysis buffer (0.05 M Tris-HCl, pH 7.5, 0.15 M NaCl, 1% NP-40, and 0.1 M PMSF) with glass beads and blotted with anti–Bcl-x_L (1:5,000 rabbit monoclonal) and anti–rabbit IgG (1:20,000; GE Healthcare).

Online supplemental material

Fig. S1 shows that no respiratory defects were detected in *bcl-x*–deficient mitochondria. Fig. S2 shows coimmunogold EM for Bcl-x_L and F_1 β subunit. Fig. S3 shows protease digestion of mitochondria detected with Bcl-x_L antibody. Fig. S4 shows an example of TMRE traces and Bcl-x_L blots for shRNA knockdowns in Fig. 4 G. Fig. S5 shows expression levels of Bcl-x_L protein in yeast. Online supplemental material is available at http://www.jcb.org/cgi/content/full/jcb.201108059/DC1.

We thank Dr. L. Boise (University of Miami, Miami, FL) for the Bcl-x_L antibody.

This work was supported by research grants GM077875 and NS37402 (to J. Marie Hardwick), R37-HL54598 (to B. O'Rourke), NS40932 (to Y.-T. Hsu), DC01919 and NS018492 (to L.K. Kaczmarek), NS045876 (to E.A. Jonas), and CA010951 (to P.L. Pedersen) from the National Institutes of Health.

Submitted: 10 August 2011
Accepted: 14 September 2011

References

Abramov, A.Y., A. Scorziello, and M.R. Duchen. 2007. Three distinct mechanisms generate oxygen free radicals in neurons and contribute to cell death during anoxia and reoxygenation. *J. Neurosci.* 27:1129–1138. http://dx.doi.org/10.1523/JNEUROSCI.4468-06.2007

Alavian, K., L. Collis, H. Li, L. Bonanni, L. Zeng, S. Sacchetti, E. Lazrove, P. Nabili, B. Flaherty, M. Graham, et al. 2011. Bcl-xL regulates metabolic efficiency of neurons through interaction with the mitochondrial F1FO ATP synthase. *Nat. Cell Biol.* In press.

Aon, M.A., S. Cortassa, E. Marbán, and B. O'Rourke. 2003. Synchronized whole cell oscillations in mitochondrial metabolism triggered by a local release of reactive oxygen species in cardiac myocytes. *J. Biol. Chem.* 278:44735–44744. http://dx.doi.org/10.1074/jbc.M302673200

Basañez, G., J.C. Sharpe, J. Galanis, T.B. Brandt, J.M. Hardwick, and J. Zimmerberg. 2002. Bax-type apoptotic proteins porate pure lipid bilayers through a mechanism sensitive to intrinsic monolayer curvature. *J. Biol. Chem.* 277:49360–49365. http://dx.doi.org/10.1074/jbc.M206069200

Bellows, D.S., M. Howell, C. Pearson, S.A. Hazlewood, and J.M. Hardwick. 2002. Epstein-Barr virus BALF1 is a BCL-2-like antagonist of the herpesvirus antiapoptotic BCL-2 proteins. *J. Virol.* 76:2469–2479. http://dx.doi.org/10.1128/jvi.76.5.2469-2479.2002

Belzacq, A.S., H.L. Vieira, F. Verrier, G. Vandecasteele, I. Cohen, M.C. Prévost, E. Larquet, F. Pariselli, P.X. Petit, A. Kahn, et al. 2003. Bcl-2 and Bax modulate adenine nucleotide translocase activity. *Cancer Res.* 63:541–546.

Benard, G., and R. Rossignol. 2008. Ultrastructure of the mitochondrion and its bearing on function and bioenergetics. *Antioxid. Redox Signal.* 10:1313–1342. http://dx.doi.org/10.1089/ars.2007.2000

Berman, S.B., Y.B. Chen, B. Qi, J.M. McCaffery, E.B. Rucker III, S. Goebbels, K.A. Nave, B.A. Arnold, E.A. Jonas, F.J. Pineda, and J.M. Hardwick. 2009. Bcl-x_L increases mitochondrial fission, fusion, and biomass in neurons. *J. Cell Biol.* 184:707–719. http://dx.doi.org/10.1083/jcb.200809060

Billen, L.P., C.L. Kokoski, J.F. Lovell, B. Leber, and D.W. Andrews. 2008. Bcl-XL inhibits membrane permeabilization by competing with Bax. *PLoS Biol.* 6:e147. http://dx.doi.org/10.1371/journal.pbio.0060147

Chau, B.N., E.H. Cheng, D.A. Kerr, and J.M. Hardwick. 2000. Aven, a novel inhibitor of caspase activation, binds Bcl-xL and Apaf-1. *Mol. Cell*. 6:31–40.

Cheng, E.H., B. Levine, L.H. Boise, C.B. Thompson, and J.M. Hardwick. 1996. Bax-independent inhibition of apoptosis by Bcl-XL. *Nature*. 379:554–556. http://dx.doi.org/10.1038/379554a0

Cheng, E.H., T.V. Sheiko, J.K. Fisher, W.J. Craigen, and S.J. Korsmeyer. 2003. VDAC2 inhibits BAK activation and mitochondrial apoptosis. *Science*. 301:513–517. http://dx.doi.org/10.1126/science.1083995

Cheng, T., J. Sudderth, C. Yang, A.R. Mullen, E.S. Jin, J.M. Matés, and R.J. DeBerardinis. 2011. Pyruvate carboxylase is required for glutamine-independent growth of tumor cells. *Proc. Natl. Acad. Sci. USA*. 108:8674–8679. http://dx.doi.org/10.1073/pnas.1016627108

Cheng, W.C., X. Teng, H.K. Park, C.M. Tucker, M.J. Dunham, and J.M. Hardwick. 2008. Fis1 deficiency selects for compensatory mutations responsible for cell death and growth control defects. *Cell Death Differ.* 15:1838–1846. http://dx.doi.org/10.1038/cdd.2008.117

Fannjiang, Y., C.H. Kim, R.L. Huganir, S. Zou, T. Lindsten, C.B. Thompson, T. Mito, R.J. Traystman, T. Larsen, D.E. Griffin, et al. 2003. BAK alters neuronal excitability and can switch from anti- to pro-death function during postnatal development. *Dev. Cell*. 4:575–585. http://dx.doi.org/10.1016/S1534-5807(03)00091-1

Fannjiang, Y., W.C. Cheng, S.J. Lee, B. Qi, J. Pevsner, J.M. McCaffery, R.B. Hill, G. Basañez, and J.M. Hardwick. 2004. Mitochondrial fission proteins regulate programmed cell death in yeast. *Genes Dev.* 18:2785–2797. http://dx.doi.org/10.1101/gad.1247904

Galindo, K.A., W.J. Lu, J.H. Park, and J.M. Abrams. 2009. The Bax/Bak ortholog in *Drosophila*, Debcl, exerts limited control over programmed cell death. *Development*. 136:275–283. http://dx.doi.org/10.1242/dev.019042

Galonek, H.L., and J.M. Hardwick. 2006. Upgrading the BCL-2 network. *Nat. Cell Biol.* 8:1317–1319. http://dx.doi.org/10.1038/ncb1206-1317

Garlid, K.D., and P. Paucek. 2003. Mitochondrial potassium transport: the K(+) cycle. *Biochim. Biophys. Acta*. 1606:23–41. http://dx.doi.org/10.1016/S0005-2728(03)00108-7

Gotow, T., M. Shibata, S. Kanamori, O. Tokuno, Y. Ohsawa, N. Sato, K. Isahara, Y. Yayoi, T. Watanabe, J.F. Leterrier, et al. 2000. Selective localization of Bcl-2 to the inner mitochondrial and smooth endoplasmic reticulum membranes in mammalian cells. *Cell Death Differ.* 7:666–674. http://dx.doi.org/10.1038/sj.cdd.4400694

Graham, S.C., M.W. Bahar, S. Cooray, R.A. Chen, D.M. Whalen, N.G. Abrescia, D. Alderton, R.J. Owens, D.I. Stuart, G.L. Smith, and J.M. Grimes. 2008. Vaccinia virus proteins A52 and B14 Share a Bcl-2-like fold but have evolved to inhibit NF-kappaB rather than apoptosis. *PLoS Pathog.* 4:e1000128. http://dx.doi.org/10.1371/journal.ppat.1000128

Hardwick, J.M., and R.J. Youle. 2009. SnapShot: BCL-2 proteins. *Cell*. 138:404–404. e1. http://dx.doi.org/10.1016/j.cell.2009.07.003

Hockenbery, D., G. Nuñez, C. Milliman, R.D. Schreiber, and S.J. Korsmeyer. 1990. Bcl-2 is an inner mitochondrial membrane protein that blocks programmed cell death. *Nature*. 348:334–336. http://dx.doi.org/10.1038/348334a0

Hong, S., and P.L. Pedersen. 2004. Mitochondrial ATP synthase: a bioinformatic approach reveals new insights about the roles of supernumerary subunits g and A6L. *J. Bioenerg. Biomembr.* 36:515–523. http://dx.doi.org/10.1007/s10863-004-8998-y

Hoppins, S., F. Edlich, M.M. Cleland, S. Banerjee, J.M. McCaffery, R.J. Youle, and J. Nunnari. 2011. The soluble form of Bax regulates mitochondrial fusion via MFN2 homotypic complexes. *Mol. Cell*. 41:150–160. http://dx.doi.org/10.1016/j.molcel.2010.11.030

Hou, Q., E. Cymbalyuk, S.C. Hsu, M. Xu, and Y.T. Hsu. 2003. Apoptosis modulatory activities of transiently expressed Bcl-2: roles in cytochrome C release and Bax regulation. *Apoptosis*. 8:617–629. http://dx.doi.org/10.1023/A:1026187526113

Hsu, Y.T., and R.J. Youle. 1997. Nonionic detergents induce dimerization among members of the Bcl-2 family. *J. Biol. Chem.* 272:13829–13834. http://dx.doi.org/10.1074/jbc.272.21.13829

Hsu, Y.T., Q. Hou, E. Cymbalyuk, and R. Youle. 2003. Generation and characterization of species-specific anti-Bcl-X(L) monoclonal antibodies. *Hybrid. Hybridomics*. 22:91–95. http://dx.doi.org/10.1089/153685903321948012

Jastroch, M., A.S. Divakaruni, S. Mookerjee, J.R. Treberg, and M.D. Brand. 2010. Mitochondrial proton and electron leaks. *Essays Biochem.* 47:53–67. http://dx.doi.org/10.1042/bse0470053

Jeong, S.Y., B. Gaume, Y.J. Lee, Y.T. Hsu, S.W. Ryu, S.H. Yoon, and R.J. Youle. 2004. Bcl-x(L) sequesters its C-terminal membrane anchor in soluble, cytosolic homodimers. *EMBO J.* 23:2146–2155. http://dx.doi.org/10.1038/sj.emboj.7600225

Kaczmarek, L.K. 1976. Frequency sensitive biochemical reactions. *Biophys. Chem.* 4:249–251. http://dx.doi.org/10.1016/0301-4622(76)80071-3

Karbowski, M., K.L. Norris, M.M. Cleland, S.Y. Jeong, and R.J. Youle. 2006. Role of Bax and Bak in mitochondrial morphogenesis. *Nature*. 443:658–662. http://dx.doi.org/10.1038/nature05111

Kharbanda, S., P. Pandey, L. Schofield, S. Israels, R. Roncinske, K. Yoshida, A. Bharti, Z.M. Yuan, S. Saxena, R. Weichselbaum, et al. 1997. Role for Bcl-xL as an inhibitor of cytosolic cytochrome C accumulation in DNA damage-induced apoptosis. *Proc. Natl. Acad. Sci. USA*. 94:6939–6942. http://dx.doi.org/10.1073/pnas.94.13.6939

Ko, Y.H., M. Delannoy, J. Hullihen, W. Chiu, and P.L. Pedersen. 2003. Mitochondrial ATP synthasome. Cristae-enriched membranes and a multiwell detergent screening assay yield dispersed single complexes containing the ATP synthase and carriers for Pi and ADP/ATP. *J. Biol. Chem.* 278:12305–12309. http://dx.doi.org/10.1074/jbc.C200703200

Kowaltowski, A.J., R.G. Cosso, C.B. Campos, and G. Fiskum. 2002. Effect of Bcl-2 overexpression on mitochondrial structure and function. *J. Biol. Chem.* 277:42802–42807. http://dx.doi.org/10.1074/jbc.M207765200

Kristian, T., N.B. Pivovarova, G. Fiskum, and S.B. Andrews. 2007. Calcium-induced precipitate formation in brain mitochondria: composition, calcium capacity, and retention. *J. Neurochem.* 102:1346–1356. http://dx.doi.org/10.1111/j.1471-4159.2007.04626.x

Lam, M., M.B. Bhat, G. Nuñez, J. Ma, and C.W. Distelhorst. 1998. Regulation of Bcl-xl channel activity by calcium. *J. Biol. Chem.* 273:17307–17310. http://dx.doi.org/10.1074/jbc.273.28.17307

Letai, A.G. 2008. Diagnosing and exploiting cancer's addiction to blocks in apoptosis. *Nat. Rev. Cancer*. 8:121–132. http://dx.doi.org/10.1038/nrc2297

Levine, B., S. Sinha, and G. Kroemer. 2008. Bcl-2 family members: dual regulators of apoptosis and autophagy. *Autophagy*. 4:600–606.

Lewis, J., G.A. Oyler, K. Ueno, Y.R. Fannjiang, B.N. Chau, J. Vornov, S.J. Korsmeyer, S. Zou, and J.M. Hardwick. 1999. Inhibition of virus-induced neuronal apoptosis by Bax. *Nat. Med.* 5:832–835. http://dx.doi.org/10.1038/10556

Li, H., Y. Chen, A.F. Jones, R.H. Sanger, L.P. Collis, R. Flannery, E.C. McNay, T. Yu, R. Schwarzenbacher, B. Bossy, et al. 2008. Bcl-xL induces Drp1-dependent synapse formation in cultured hippocampal neurons. *Proc. Natl. Acad. Sci. USA*. 105:2169–2174. http://dx.doi.org/10.1073/pnas.0711647105

Matsuyama, S., Q. Xu, J. Velours, and J.C. Reed. 1998. The mitochondrial F0F1-ATPase proton pump is required for function of the proapoptotic protein Bax in yeast and mammalian cells. *Mol. Cell*. 1:327–336. http://dx.doi.org/10.1016/S1097-2765(00)80033-7

McCaffery, J.M., and M.G. Farquhar. 1995. Localization of GTPases by indirect immunofluorescence and immunoelectron microscopy. *Methods Enzymol.* 257:259–279. http://dx.doi.org/10.1016/S0076-6879(95)57031-4

Montessuit, S., S.P. Somasekharan, O. Terrones, S. Lucken-Ardjomande, S. Herzig, R. Schwarzenbacher, D.J. Manstein, E. Bossy-Wetzel, G. Basañez, P. Meda, and J.C. Martinou. 2010. Membrane remodeling induced by the dynamin-related protein Drp1 stimulates Bax oligomerization. *Cell*. 142:889–901. http://dx.doi.org/10.1016/j.cell.2010.08.017

Motoyama, S., M. Kitamura, S. Saito, Y. Minamiya, H. Suzuki, R. Saito, K. Terada, J. Ogawa, and H. Inaba. 1998. Bcl-2 is located predominantly in the inner membrane and crista of mitochondria in rat liver. *Biochem. Biophys. Res. Commun.* 249:628–636. http://dx.doi.org/10.1006/bbrc.1998.9205

Narendra, D., A. Tanaka, D.F. Suen, and R.J. Youle. 2008. Parkin is recruited selectively to impaired mitochondria and promotes their autophagy. *J. Cell Biol.* 183:795–803. http://dx.doi.org/10.1083/jcb.200809125

Nicholls, D.G., and S.J. Ferguson. 2002. Bioenergetics 3. Academic Press, San Diego, CA. 297 pp.

Nicolis, G., and I. Prigogine. 1977. Self-organization in Nonequilibrium Systems: From Dissipative Structures to Order Through Fluctuations. Wiley, New York. 491 pp.

Oltersdorf, T., S.W. Elmore, A.R. Shoemaker, R.C. Armstrong, D.J. Augeri, B.A. Belli, M. Bruncko, T.L. Deckwerth, J. Dinges, P.J. Hajduk, et al. 2005. An inhibitor of Bcl-2 family proteins induces regression of solid tumours. *Nature*. 435:677–681. http://dx.doi.org/10.1038/nature03579

O'Neill, J.W., M.K. Manion, B. Maguire, and D.M. Hockenbery. 2006. BCL-XL dimerization by three-dimensional domain swapping. *J. Mol. Biol.* 356:367–381. http://dx.doi.org/10.1016/j.jmb.2005.11.032

Paumard, P., J. Vaillier, B. Coulary, J. Schaeffer, V. Soubannier, D.M. Mueller, D. Brèthes, J.P. di Rago, and J. Velours. 2002. The ATP synthase is involved in generating mitochondrial cristae morphology. *EMBO J.* 21:221–230. http://dx.doi.org/10.1093/emboj/21.3.221

Rak, M., S. Gokova, and A. Tzagoloff. 2011. Modular assembly of yeast mitochondrial ATP synthase. *EMBO J.* 30:920–930. http://dx.doi.org/10.1038/emboj.2010.364

Rosenthal, R.E., F. Hamud, G. Fiskum, P.J. Varghese, and S. Sharpe. 1987. Cerebral ischemia and reperfusion: Prevention of brain mitochondrial

injury by lidoflazine. *J. Cereb. Blood Flow Metab.* 7:752–758. http://dx.doi.org/10.1038/jcbfm.1987.130

Schwartz, P.S., M.K. Manion, C.B. Emerson, J.S. Fry, C.M. Schulz, I.R. Sweet, and D.M. Hockenbery. 2007. 2-Methoxy antimycin reveals a unique mechanism for Bcl-x(L) inhibition. *Mol. Cancer Ther.* 6:2073–2080. http://dx.doi.org/10.1158/1535-7163.MCT-06-0767

Soane, L., Z.T. Siegel, R.A. Schuh, and G. Fiskum. 2008. Postnatal developmental regulation of Bcl-2 family proteins in brain mitochondria. *J. Neurosci. Res.* 86:1267–1276. http://dx.doi.org/10.1002/jnr.21584

Teng, X., W.C. Cheng, B. Qi, T.-X. Yu, K. Ramachandran, M.D. Boersma, T. Hattier, P.V. Lehmann, F.J. Pineda, and J.M. Hardwick. 2011. Gene-dependent cell death in yeast. *Cell Death Dis*. 2:e188. http://dx.doi.org/10.1038/cddis.2011.72

Twig, G., A. Elorza, A.J. Molina, H. Mohamed, J.D. Wikstrom, G. Walzer, L. Stiles, S.E. Haigh, S. Katz, G. Las, et al. 2008. Fission and selective fusion govern mitochondrial segregation and elimination by autophagy. *EMBO J.* 27:433–446. http://dx.doi.org/10.1038/sj.emboj.7601963

Vander Heiden, M.G., X.X. Li, E. Gottleib, R.B. Hill, C.B. Thompson, and M. Colombini. 2001. Bcl-xL promotes the open configuration of the voltage-dependent anion channel and metabolite passage through the outer mitochondrial membrane. *J. Biol. Chem.* 276:19414–19419. http://dx.doi.org/10.1074/jbc.M101590200

van Raaij, M.J., J.P. Abrahams, A.G. Leslie, and J.E. Walker. 1996. The structure of bovine F1-ATPase complexed with the antibiotic inhibitor aurovertin B. *Proc. Natl. Acad. Sci. USA*. 93:6913–6917. http://dx.doi.org/10.1073/pnas.93.14.6913

Vergun, O., T.V. Votyakova, and I.J. Reynolds. 2003. Spontaneous changes in mitochondrial membrane potential in single isolated brain mitochondria. *Biophys. J.* 85:3358–3366. http://dx.doi.org/10.1016/S0006-3495(03)74755-9

Walker, J.E., and V.K. Dickson. 2006. The peripheral stalk of the mitochondrial ATP synthase. *Biochim. Biophys. Acta*. 1757:286–296. http://dx.doi.org/10.1016/j.bbabio.2006.01.001

White, C., C. Li, J. Yang, N.B. Petrenko, M. Madesh, C.B. Thompson, and J.K. Foskett. 2005. The endoplasmic reticulum gateway to apoptosis by Bcl-X(L) modulation of the InsP3R. *Nat. Cell Biol.* 7:1021–1028. http://dx.doi.org/10.1038/ncb1302

Yi, C.H., H. Pan, J. Seebacher, I.-H. Jang, S.G. Hyberts, G.J. Heffron, M.G. Vander Heiden, R. Yang, F. Li, J.W. Locasale, et al. 2011. Metabolic regulation of protein N-alpha-acetylation by Bcl-xL promotes cell survival. *Cell*. 146:607–620. http://dx.doi.org/10.1016/j.cell.2011.06.050

Youle, R.J., and A. Strasser. 2008. The BCL-2 protein family: opposing activities that mediate cell death. *Nat. Rev. Mol. Cell Biol.* 9:47–59. http://dx.doi.org/10.1038/nrm2308

Chen et al., http://www.jcb.org/cgi/content/full/jcb.201108059/DC1

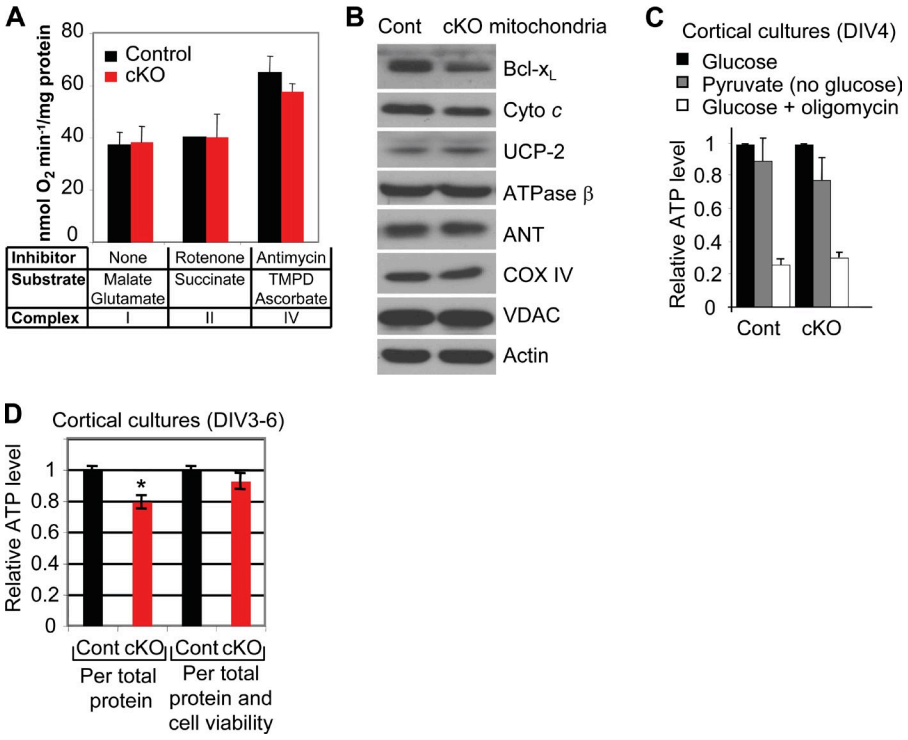

Figure S1. **No defects in *bcl-x*–deficient mitochondria under normal conditions.** (A) 1 mM ADP-stimulated rates of oxygen consumption were determined for mitochondria isolated from the cerebral cortex of P5–7 control and cKO of mouse pups (5 mM malate, 5 mM glutamate, 2.5 mM succinate, 0.5 mM tetramethylphenylenediamine [TMPD], and 2 mM ascorbate) with the indicated inhibitors for the relevant upstream complex (complex I, 2 mM rotenone; complex III, 1 mM antimycin). (B) Immunoblots of mitochondria isolated from dissected P5–7 cerebral cortex (where interneurons and glia still express Bcl-x_L). Cortices from four *bcl-x* cKO and two control (Cont) mice were pooled, and equal protein was loaded based on the BCA assay and analyzed using antibodies to ANT (sc-9299 [1:1,000; Santa Cruz Biotechnology, Inc.]), ATP synthase β subunit (1:1,000; Invitrogen), and other proteins as described in Fig. 2 A. A representative of three independent experiments is shown. VDAC, voltage-dependent anion channel. Molecular mass is indicated in kilodaltons. (C) Relative contributions of mitochondria and glycolysis to whole-cell ATP levels. Cortical neurons cultures (DIV4) were transferred to medium containing 25 mM glucose, glucose-free medium supplemented with 10 mM pyruvate to fuel mitochondria, or medium containing 25 mM glucose and 5 mg/ml of ATP synthase inhibitor oligomycin for 1 h and were then harvested for total ATP determination for each culture dish using a bioluminescence assay (Invitrogen). The absolute value of ATP was calculated from a standard curve generated for each individual experiment using fresh ATP standards (0 nM, 5 nM, 50 nM, 500 nM, 5 µM, and 25 µM) and was normalized by the protein content of each individual sample by BCA assay. Samples were analyzed immediately, or all time points were frozen instantly and analyzed together. Data are presented for three independent experiments, each with two to four different cultures/samples per genotype (control, $n = 9$; cKO, $n = 10$). A *t* test was used; all comparisons were not significantly different ($p > 0.13$). (D) Total ATP levels in cortical neuron cultures (DIV3–6). The mean value for cKO cultures was determined proportional to control and the results from multiple samples (control, $n = 18$; cKO, $n = 19$) in seven independent experiments (left). Relative ATP values for the same cortical cultures were further normalized by the mean difference in cell viability per experiment (mean ratio of cell viability for control/cKO = 1:0.85), determined by nuclear morphology using Hoechst (right). Data are presented as the mean ± SEM. The p value (*, $P < 0.0002$) was determined using a *t* test.

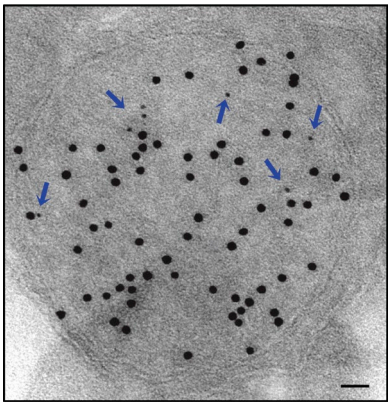

Figure S2. **Cryo-EM of *bcl-x*$^{+/+}$ mouse brain confirms mitochondrial matrix localization of endogenous Bcl-x_L protein.** An example of a mitochondrion co-labeled by immunogold for the β subunit of the ATP synthase (large gold beads) and Bcl-x_L (small gold; arrows) is shown. Note that the size of the antibody–bead complex will not permit colabeling of the same protein complex. Bar, 0.1 mm.

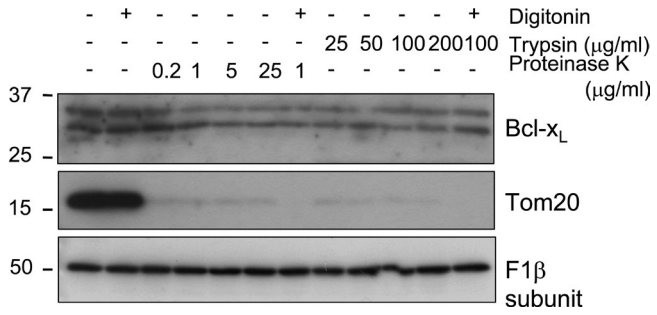

Figure S3. **Protease digestion of mitochondria detected with Bcl-x_L antibody.** Bcl-x_L is protected from protease digestion after permeabilization of the outer mitochondrial membrane of isolated rat brain mitochondria with digitonin. The blotting was performed as described for Fig. 2 E, except with anti–Bcl-x_L antibody. Molecular mass is indicated in kilodaltons.

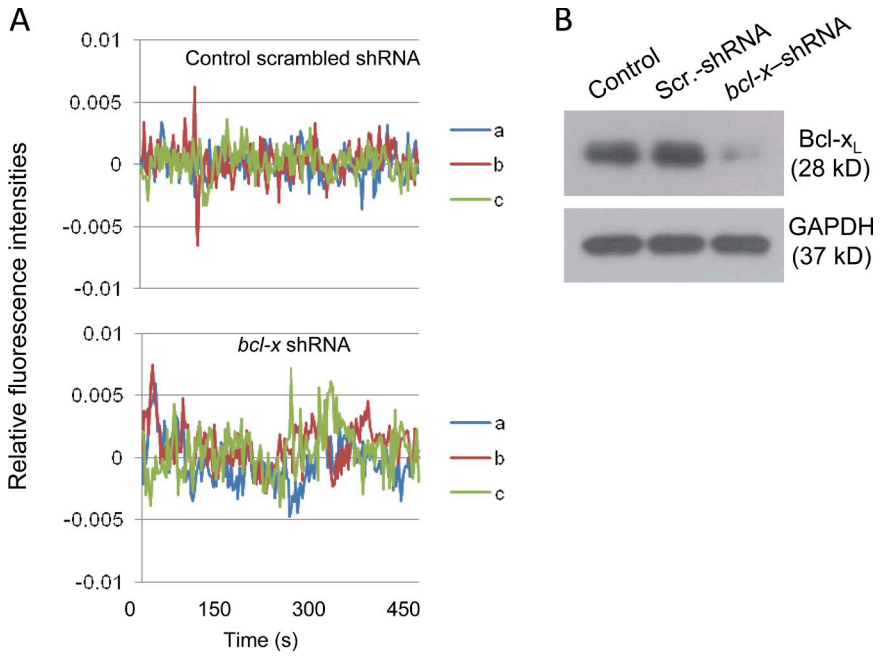

Figure S4. **Example of TMRE traces and Bcl-x_L blots for shRNA knockdowns.** (A) Fluorescence traces for three mitochondria per condition used to calculate SDs shown in Fig. 4 G. (B) Immunoblot analysis verifying shRNA knockdown of Bcl-x_L in hippocampal neurons results in Fig. 4 G. Lentivirus plasmids (pGIPZ vector) express the following shRNAs against rat BCL-x_L: 5′-CGGGCTCACTCTTCAGTCGGAATAGTGAAGCCACAGATGTATTCCGACTGAAGAGT-GAGCCCA-3′ or scrambled (Scr.) control (cat# RHS4346; Thermo Fisher Scientific). GAPDH, glyceraldehyde 3-phosphate dehydrogenase.

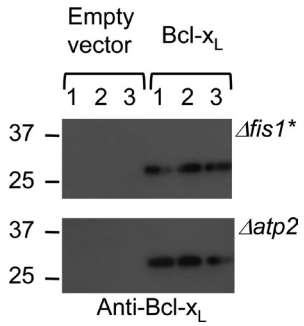

Figure S5. **Immunoblots of human Bcl-x_L in yeast cell lysates.** Three independently transformed strains for each plasmid in each of the indicated yeast knockout strains are shown. Molecular mass is indicated in kilodaltons.